

GEOMETRIC AND MATERIAL NONLINEAR EFFECTS IN
ELASTIC-PLASTIC AND FAILURE ANALYSES OF ANISOTROPIC
LAMINATED STRUCTURES

by

Dave Rourk

Dissertation submitted to the Faculty of the
Virginia Polytechnic Institute and State University
in partial fulfillment of the requirements
for the degree of

Doctor of Philosophy

in

Engineering Mechanics

APPROVED:

J. N. Reddy, Chairman

D. Frederick

E. G. Henneke, II

T. Kuppusamy

A. C. Loos

December, 1986
Blacksburg, Virginia

GEOMETRIC AND MATERIAL NONLINEAR EFFECTS IN
ELASTIC-PLASTIC AND FAILURE ANALYSES OF ANISOTROPIC
LAMINATED STRUCTURES

by

Dave Rourk
Department of Engineering Science and Mechanics
Virginia Polytechnic Institute and State University

(ABSTRACT)

In this study, an analytical procedure to predict the strength and failure of laminated composite structures under monotonically increasing static loads is presented. A degenerated 3-D shell finite element that includes linear elastic and plastic material behavior with full geometric nonlinearity is used to determine stresses at selected points (Gauss quadrature points in each element) of the structure. Material stiffness (constitutive) matrices are evaluated at each Gauss point, in each lamina and in each element, and when the computed stress state violates a user selected failure criterion, the material stiffness matrix at the failed Gauss point is reduced. The reduction procedure involves setting the material stiffnesses to unity. Examples of isotropic, orthotropic, anisotropic and composite laminates are presented to illustrate the validity of the procedure developed and to evaluate various failure theories. Maximum stress, modified Hills (Mathers), Tsai-Wu ($F_{12} = 0$), and Hashin's failure criteria are included.

The results indicate that for large length-to-thickness ratios, the geometric nonlinear effect should be incorporated for both isotropic and anisotropic structures. The nonlinear material model influences the

behavior of isotropic structures with small length-to-thickness ratios, while having nearly no effect at all on laminated anisotropic structures. Of the four failure theories compared, each predicts failure at nearly the same load levels and locations. Hashin's criterion is particularly noteworthy in that the mode is also predicted.

Acknowledgements

The author would like to express his heartfelt thanks to Professors Reddy, Frederick, Henneke, Kuppusamy and Loos for their encouragement and support throughout this project.

The monetary support of this research by the Mechanics Division of the Office of Naval Research and the Mathematical Sciences Section of the Army Research Office is gratefully acknowledged.

*To the courage to go beyond where you thought you could go,
and especially to those who inspire that courage within each
of us.*

TABLE OF CONTENTS

	Page
CHAPTER 1. INTRODUCTION.....	1
1.1 Preliminary Comments.....	1
1.2 Objective of the Present Study.....	3
1.3 Background Literature.....	4
CHAPTER 2. GOVERNING EQUATIONS.....	18
2.1 Incremental Form of the Equilibrium Equations.....	18
2.2 Finite Element Geometry and Formulation.....	21
2.3 Material Nonlinearity.....	30
2.4 Computational Procedure.....	37
2.5 Assumptions and Procedures Used in the Program.....	40
2.6 Reducing Stress States to the Plasticity Functions Surface.....	42
CHAPTER 3. NUMERICAL RESULTS.....	46
3.1 Isotropic Thick Plate.....	46
3.2 Orthotropic and Cross Ply Thin Plate.....	48
3.3 Isotropic Cylindrical Shell.....	48
3.4 Isotropic Spherical Shell.....	48
3.5 Combined Geometric and Material Nonlinearities.....	51
3.6 Plate Strip.....	55
3.6.1 Isotropic Plate Strip.....	55
3.6.2 Orthotropic Plate Strip.....	57
3.6.3 Cross-Ply Plate Strip.....	64
3.6.4 Angle Ply (45°/-45°) Plate Strip.....	66
CHAPTER 4. SUMMARY AND DISCUSSION.....	70
4.1 General Comments.....	70
4.2 Geometric and Material Nonlinear Effects.....	71
4.3 Failure Criteria.....	71
4.4 Recommendations.....	72
CHAPTER 5. References.....	74
Appendix A: Material Properties Used in this Study.....	80
Vita.....	83

CHAPTER 1

INTRODUCTION

1.1 Preliminary Comments

The ability to predict the behavior of a laminated, composite structure beyond the first-ply failure is important in the preliminary and final design of structures. Also, the prediction of how the strength of a structure decreases under applied loads can be of great help to designers and engineers.

Today, it is routine to do most structural analyses using the finite element method. By far, the elements most frequently used in common structural problems are based on plate or shell theories. To keep up with the recent developments in the use of composite materials, these elements have been modified to include the variation of stresses and strains through the thickness of the laminate. The plate and shell theories are two-dimensional approximations of the 3-D elasticity theory, and these theories do not account for the changes in geometry during deformation. Three-dimensional elements based on the 3-D elasticity theory become impractical to use in laminated structures because at least one element would be required to model each lamina of a laminate, and then, keeping within a reasonable aspect ratio of element length to thickness, many elements would be required to model any laminate.

A compromise between the elements based on plate or shell theory and the three-dimensional elements in modelling a laminate is a degenerated three-dimensional (3-D) shell or plate element. The 3-D

degenerated element is based on the three-dimensional elasticity equations with three assumptions; 1) a line straight and normal to the middle surface before deformation remains straight, but not necessarily normal to the middle surface, after deformation, 2) the strain energy from the stresses perpendicular to the middle surface are ignored, and 3) the shell thickness-to-curvature ratio is small. The first assumption allows the modeling of shear deformation, important in thick shells. The second assumption improves the numerical conditioning of the element since these strain energies are generally small compared to the others, and the third assumption implies that derivatives at either end of a middle surface normal line of the shell with respect to the shell coordinates are the same. Therefore, the Jacobian matrix is free of the through-the-thickness coordinate and numerical integration need only be performed in the surface of the shell.

With the stress-strain information in hand, the problem of defining how the material fails requires a criterion based on physical considerations. There have been many failure criteria proposed for anisotropic materials, and a review is presented in Section 1.3. If a set of failure criteria were at hand, and a classification of material systems to failure criteria existed, then the designer or engineer could simply choose the particular failure criterion that went with the material system the structure was to be made from. While this classification doesn't exist per se, an intelligent choice of several failure criteria can be made from knowing some basic information about the material system used.

1.2 Objective of the Present Study

The overall objective of the present study is to develop a computational procedure to predict failure in laminated anisotropic structures composed of orthotropic laminae, and to determine the strength reduction due to an applied static load. In the interest of utilizing the high strength and stiffness of composite materials the stress states within these materials will be pushed to higher levels causing plastic material behavior in addition to possible geometric nonlinearities.

Three major tasks are to be completed in order to achieve the objective:

1. The 3-D degenerated element must be extended to include material non-linearity in composite laminates. This will be done using an associated flow rule with isotropic work hardening (that is, the hardening will be incorporated into the yield function by equating plastic work done in different stress directions). This is the mechanism that will reduce stiffnesses at plastically stressed points in the structure.
2. The failure criteria must be incorporated into the computational scheme. Since the loading will be iterative, a given failure criterion must be checked at each Gauss point, and at each load level, for each element. This will signal where in the structure the lamina properties are to be reduced.
3. A comparison of the failure predictions of several failure criteria when applied to an anisotropic structure undergoing geometric and material nonlinear behavior will be undertaken.

After these steps are completed, an analytical method for predicting where, and in what mode (shear, tensile, compressive), failure will occur in a composite structure will be available.

1.3 Background Literature

The application of the finite element method to the analysis of laminated composite shells, including geometric and material nonlinearities is relatively a recent occurrence (see [1-10]). The composite laminates are treated as an equivalent single layer [3] or as a degenerated 3-D continuum [1,2]. The geometric nonlinearity used in single-layer theories is one of the von Karman type, whereas the full nonlinearity is used in the degenerated 3-D theories. The material nonlinearity has been approached from either the micromechanics or macromechanics points of view.

Micromechanics Models

In the micromechanics approach, the matrix is considered as an elastic-plastic material while the fibers are considered to be brittle-elastic. An elastic-plastic continuum model for fiber reinforced composites was developed by Mulhern, Rogers and Spencer [11]. In this model the composite material is treated as transversely isotropic, with inextensible fibers and a rigid-perfectly plastic matrix. The yield surface was formulated in terms of invariants characteristic of the transversely isotropic geometry. The extension of an elastic fiber with an elastic-perfectly plastic coating was considered by Mulhern et al. [12]. The stages of development of the plastic zone in the fiber coating was examined. These were compared to the results obtained by

Hill [13]. Hill's solution differed in that the fiber coating yielded instantaneously. The two solutions essentially agreed. In a later publication [14], Mulhern et al. extended their earlier continuum theory [11] to include an elastic fiber and an elastic-perfectly plastic matrix. The assumed yield function was unaffected by normal stress in the fiber direction, this eliminated the prediction of hysteresis loops found in their earlier work [12]. Spencer [15] extended this theory to a composite reinforced by two families of fibers. This was useful in studying the behavior of composite laminates. The same model was used in other applications, such as the dynamic analysis of composite beams [16] and large deformation of composite structures [17,18].

Dvorak and his colleagues [19-28] have been active for many years in the development of constitutive models for metal matrix composites. One of their earlier works [19] used the finite element method to establish the initial yield surface of a metal matrix composite assuming a hexagonal fiber array. These results were later generalized [30] by introducing a set of stress invariants characteristic of the transversely isotropic geometry. The initial yield surface was found to be an irregular ellipsoid with its longest axis inclined toward the hydrostatic stress axis. Their analysis showed the matrix yielding generally starts at the fiber-matrix interface. The yielding was influenced in the fiber direction by the fiber to matrix moduli ratio and the fiber volume fraction. Transverse to the fiber, the initial yielding was controlled by the matrix yield stress. Hydrostatic stress was shown to cause yielding and volume changes, unlike typical metal behavior. Relatively small temperature changes were shown to produce

matrix yielding. Values as small as 70° F were shown to cause initial yielding for a boron/aluminum composite with a 10,000 psi matrix yield stress. Based upon their investigation of initial yield surfaces, Dvorak and Rao [21] developed a simple but accurate continuum plasticity theory for axisymmetric deformation of unidirectional fibrous composites. Assuming elastic fibers with a nonhardening matrix, a simple hardening rule and associated flow rule was formulated. In comparison with a composite cylinder model evaluated by the finite element method for a complex load history, the continuum theory showed very good agreement. Their axisymmetric theory, also applied to the problem of analyzing uniform temperature changes in a metal matrix composite, showed considerable success [22].

The elastic-plastic behavior of fibrous composites was explored by Dvorak and Bahei-El-Din [23] using the self-consistent micromechanics scheme [13]. The authors modified the scheme to alleviate the problems reported by Hutchinson [29], who observed high estimates of initial yield stress and low plastic strains in the early stages of deformation. To correct this problem, the authors replaced the elastic inclusion by a composite cylinder model of Dvorak and Rao [21]. For the case of axisymmetric mechanical loading, the modified self-consistent model produced similar results to the unmodified self-consistent model and the composite cylinder model. The authors examined the case of initial yield due to longitudinal shear loading, the modified self-consistent model performed well while the unmodified self-consistent model encountered some difficulties. Calculations of longitudinal shear loads gave an initial yield stress which was substantially higher than the

matrix yield stress. This contradicts initial yield estimates obtained by the finite element analysis [20], which showed the initial yield stress well below the matrix yield stress. The modifications to the self-consistent model were found to improve the performance, yet they were found to be prohibitively difficult for nonsymmetric loading.

In order to obtain a general constitutive model and retain computational simplicity, Dvorak and Bahei-El-Din [24,30] introduced a simple micromechanics model which they called the Vanishing Fiber Diameter Model. In this model it was assumed that each of the cylindrical fibers have a vanishing diameter while the fiber volume fraction in the composite remains finite. In effect the fiber imposes a constraint on the matrix in the longitudinal direction. The simplicity of this model allows for the easy incorporation of any matrix material nonlinearity. This was demonstrated by Lou and Schapery [31] in which a nonlinear viscoelastic material model was used in conjunction with a similar model. Bahei-El-Din [25-30] incorporated the Vanishing Fiber Diameter model with a Mises-type matrix material which obeys the Prager-Ziegler kinematic hardening rule. This constitutive model was used in classical lamination theory and a three-dimensional finite element analysis code called PAC78. In order to obtain good correlation with experimental results, Bahei-El-Din resorted to using in-situ matrix properties, since the unreinforced matrix properties yielded poor results. Initial yield surfaces computed for a cross-ply laminate showed reasonable agreement compared to results obtained by a finite element computation from Rao [32]. Experimental results for a cyclically loaded laminate were compared to the results from PAC78

[28]. The predicted strains in the load direction showed very good agreement. The strains in the unloaded direction were over-estimated. The authors suggest the discrepancy could be a result of neglecting the fiber-matrix constraint in the transverse direction.

Hoffman [33] developed a plane stress initial yield criterion for metal matrix composites based upon the concept of partial stresses. The partial stress concept is based on the stress in the laminate satisfying equilibrium and compatibility. The equilibrium condition is that the total stress is equal to the sum of the matrix and the fiber stresses, and the compatibility condition requires that the strains in the matrix and the fiber are identical. Retaining only the axial fiber stiffness, Hoffman then obtained a very simple expression for the Mises' yield condition in terms of the matrix stresses. Min [34], using Hoffman's partial stress model, developed an elastic-plastic material model which incorporated a kinematic hardening rule similar to that of Bahei-El-Din and Dvorak [27] for a nonhardening matrix material. Min and Crossman [35] used a plane stress mechanics of materials model for the elastoplastic deformation analysis of unidirectional composites subjected to both thermal and mechanical loading. The model explicitly accounts for the microstresses and the thermal residual stresses but only for a nonhardening matrix. The model of Min and Crossman was extended by Min and Flagg [36,37] by adding a White-Besseling plasticity model [38] for the matrix material. The resulting constitutive model was incorporated into a nonlinear laminate analysis program. The nonlinear system of equations obtained in the laminate analysis was solved by a modified Newton method with a line search

[39]. The thermal cycling-induced deformations of a unidirectionally reinforced graphite/magnesium composite were examined by Wolf, Min and Kural [40], who used the mechanics of material model developed by Min and Flagg [36,37] to analyze the complex thermal load history. The comparison was poor. Explanations for the behavior were attributed to the temperature dependence of the matrix yield stress (which was ignored in the analysis) and the presence of matrix creep.

Ruffin, Rimbois and Bigelow [41] developed an elastic-plastic point stress laminate analysis program called MLAP. Their program was formulated using the Vanishing Fiber Diameter model and a kinematic hardening Mises-type matrix material based upon Dvorak and Bahei-El-Din [25,28]. Comparison of experimental results and predictions by MLAP showed fair agreement. Program MLAP over-predicted the transverse strains, which seems to be characteristic of the micromechanics formulation [28]. The authors used unreinforced matrix material properties; possibly their results could have been improved by using in-situ properties like Dvorak and Bahei-El-Din [28].

Aboudi, in a series of papers [42-45], developed a continuum model for fiber reinforced elastic-viscoplastic composites. The theory is formulated for a viscoplastic matrix with transversely isotropic or viscoplastic fiber. The unidirectional fibers were assumed to have rectangular cross sections and were arranged in a doubly periodic rectangular array. This geometry allowed the use of Legendre polynomials for the expansion of the displacement field within each sub-cell. The solution was obtained by imposing displacement and stress continuity at the sub-cell interfaces and appropriate boundary

conditions on the unit cell. The author obtained a first order solution to his general theory and demonstrated excellent agreement for the elastic case with other micromechanics solutions. Comparisons with experimental results also showed good agreement. The transverse and shear moduli results were particularly promising. No viscoplastic computations were compared with experimental results. This would have made it possible to assess the relative performance of Aboudi's model to the Vanishing Fiber Diameter model of Dvorak. Several examples of the viscoplastic behavior were compared to available finite element solutions, and good agreement was demonstrated.

Macromechanics Models

One of the first attempts at analyzing the nonlinear behavior of composites at the macromechanics level was performed by Petit and Waddoups [46]. The authors considered the nonlinearities uncoupled in the longitudinal, transverse and shear directions which acted independently during combined loading. Failure of individual plies were determined by a maximum strain criterion. The authors made certain assumptions upon the behavior of the failed plies. Transverse ply failure implied that load could still be carried in the longitudinal or shear directions. Similarly, shear failure implied that load could still be carried in the longitudinal or transverse directions. Longitudinal failure, however, implied a total ply failure and no further load carrying capability. The authors incorporated these principles into a laminate analysis program. The plies were allowed successive failures until the laminate ultimately failed. The

correlation to experimental results for stress-strain response was fair to good, but the failure predictions were generally poor.

Hahn and Tsai [47] modeled nonlinear shear response of a composite by introducing a complementary elastic energy density function. A polynomial expansion of the complementary elastic energy density function was performed. In addition to the second order terms which describe the linear elastic behavior, one fourth-order term was retained to describe the nonlinear shear behavior. The application of this model to unidirectional (see Hahn and Tsai [47]) and multidirectional composite systems (see Hahn [48]) produced fair results.

The anisotropic plasticity theory of Hill [49,50,32] has inspired many subsequent researchers to develop constitutive models. Hill originally proposed his theory to model the weakly orthotropic behavior typically found in cold rolled metals. In this theory it is assumed that yielding is independent of hydrostatic stress and plastic flow is incompressible. Several authors have suggested extension to Hill's theory. Hu [41] and Jensen, et al [42] proposed work hardening rules. Dubey and Hiller [53] developed a more general yield criterion which was an associated flow rule based upon invariant principles. Shih and Lee [54] formulated a simple extension which allows distortion of the yield surface and variations of the anisotropic yield parameters during deformation.

Pifko, Levine and Armen [55] developed a three-dimensional finite element program for the inelastic analysis of composites. Heuristic arguments were used to develop a simple normality condition and kinematic hardening rule. Renieri and Herakovich [56] used quasi three-

dimensional finite element analysis to examine the thermomechanical response of composite laminates. In their analysis, nonlinear material behavior was introduced by a Ramberg-Osgood expression for material properties, but no interaction was assumed. Griffin, Kamat and Herakovich [57] used Hill's anisotropic plasticity theory and modification proposed by Shih and Lee [54] to develop a finite element program. Analysis of the nonlinear response of unidirectional off-axis composites showed generally good agreement.

Even with today's computers, when overall response of a structure is desired, one is forced to use a macromechanical approach. In 1969, Whang [6] considered the elasto-plastic finite element analysis of orthotropic plates and shells using strain hardening parameters. In 1974, Valliappan, Boonlualohr and Lee [10] used the modified Von Mises yield function and the associated flow rule, retaining the inplane stress components, to study materially non-linear laminate behavior. More recently, Owen and Figueiras [7] used the semi-loof element study the problem, Chandrashekhara and Reddy [3] developed a 2-D shell element that included the transverse shear stresses and the modified Von Mises yield function with the inplane interaction term.

The review of the literature indicates that the 3-D degenerate finite element, based on the three-dimensional elasticity theory, is not used to model elastic-plastic behavior and failure of composite structures. This motivated the present study. A brief review of the literature on the 3-D degenerated element is presented next.

3-D Degenerated Shell Element

Large deflection analyses of laminated composite shells are not prevalent in the literature. In 1981, Chang and Sawamiphakdi [1] used the updated Lagrangian description in their formulation of a 3-D degenerated element for geometrically non-linear bending analysis of a laminated shell. Chao and Reddy [2] have made the latest effort in this area when they used the total Lagrangian representation in their formulation of a transient, geometrically non-linear, 3-D degenerated element for laminated shells. Good correlation between several test cases and experimental data were presented making the conclusion that their model is indeed accurate. Mentioned in the conclusion of Chao and Reddy's paper, is the fact that adding material nonlinearity should enhance the element's accuracy and application to structures undergoing large deformation, including plasticity.

Failure Theories

Another objective of this study is to compare different failure criteria for laminated, anisotropic materials using the stress information from a continuum based element. There are many different anisotropic failure criteria in the literature, and what follows is a brief, and not necessarily complete, outline of some of the most widely used failure theories.

In 1948, Hill [58] proposed a failure theory for anisotropic materials that was an extension of Von Mises's distortional energy for isotropic materials. Seventeen years later, Tsai [59] modified Hill's theory for application to orthotropic laminae composed of unidirectional

fibers assuming a plane of transverse isotropy exists perpendicular to the fiber direction. A more recent modification of Hill's theory for fibrous composites, in which transverse isotropy is not assumed, has been shown by Mathers [60]. In addition, this modified version degenerates very nicely from the three-dimensional case to the two-dimensional case, and, if the material is isotropic, this criterion collapses into the Von Mises criterion.

Another approach to the prediction of failure in laminated, anisotropic materials is the use of the tensor polynomial criterion. Tsai and Wu [61] developed a second order theory based on the work from Goldenblat and Kopnov's complex stress state paper [62]. Tennyson [63] extended the tensor polynomial to include a third term.

Among other failure criteria, there are the maximum stress and maximum strain failure theories that were extended for unidirectional fiber reinforced composites. Another interesting failure theory which treats the laminate as a whole while still considering the laminae through "interaction factors" was proposed by Puppo and Evenson [64]. Hashin [65] proposed a criterion based on the invariants of the stress tensor whereby he predicts the mode of failure. Tensile or compressive, fiber or matrix failures are allowed in this criterion.

The statistical variation of the strength parameters, ineffective length arguments, and all other micromechanical effects are assumed to be represented by the average strengths of a material. Most failure criteria use these average material strengths to predict failure. The definition of failure varies and can be defined by the strengths one chooses to use. For example, if failure is defined to be yielding, the

strengths used would be those that correspond to the stress levels at yield for the material.

In general, the strengths given for composite materials are those obtained at the ultimate stress state. At these stress levels, material nonlinearity can play an important role, especially in shear, hence the need to include this effect in the element.

Each of the anisotropic failure criteria has some drawbacks. A major drawback of the Hill type criteria is that linear stresses do not appear. The interaction term in the tensor polynomial is not easily obtained with reliability. The maximum stress and maximum strain theories present cusps that have no physical interpretation.

Arguments have been made for and against each failure criterion. Indeed, an argument about using any macroscopic failure criterion without a microscopic basis can be rightly put forth, but is practically defended because of lack of experimental evidence. In this study, the Tsai-Wu tensor polynomial, the Mather-Hill theory, Hashin's mode criterion, and the maximum stress theory will be evaluated.

The tensor polynomial is chosen because of its inherent logic; somewhere in stress space there exists a surface where failure will occur when the stress vector due to some loading intersects it. The form used in this study is,

$$F_1\sigma_{11} + F_2\sigma_{22} + F_{11}(\sigma_{11})^2 + F_{22}(\sigma_{22})^2 + F_{66}(\sigma_{66})^2 + F_{44}(\sigma_{44})^2 + F_{55}(\sigma_{55})^2 = 1 \quad (1.1)$$

where F_i , F_{ij} are strength parameters and σ_{ij} are the stress components. Hill's theory, as modified by Mathers, where direct stresses were used instead of the difference of stresses, is the second

failure criterion to be evaluated :

$$(F_1\sigma_{12})^2 + (F_2\sigma_{22})^2 - F_1F_2\sigma_{11}\sigma_{22} + (F_6\sigma_{66})^2 + (F_4\sigma_{44})^2 + (F_5\sigma_{55})^2 = 1. \quad (1.1)$$

This theory is also used, in a different form, as a yield function in this study for the elastic-plastic analysis. The only modification made to this theory is that the stress components will be checked for tension and compression and the corresponding strengths will be used.

The third failure criterion is the one proposed by Hashin [65]. He used the invariants of the stress tensor and decided only four modes of failure could be physically detected; tensile or compressive, fiber or matrix failure.

Tensile fiber failure ($\sigma_{11} > 0$)

$$1 = \left(\frac{\sigma_{11}}{F_{11}}\right)^2 + \frac{(\sigma_{12})^2 + (\sigma_{13})^2}{(F_{12})^2} \quad (1.3a)$$

Compressive fiber failure ($\sigma_{11} < 0$):

$$1 = \frac{\sigma_{11}}{(-F_{11})} \quad (1.3b)$$

Tensile Matrix Failure ($\sigma_{22} > 0$):

$$\left(\frac{\sigma_{22}}{F_{22}}\right)^2 + \left(\frac{\sigma_{23}}{F_{23}}\right)^2 + \frac{(\sigma_{12})^2 + (\sigma_{13})^2}{(F_{12})^2} = 1 \quad (1.3c)$$

Compressive matrix failure ($\sigma_{22} < 0$):

$$1 = -\frac{\sigma_{22}}{F_{22}} \left[\left(\frac{F_{12}}{F_{23}}\right)^2 \frac{1}{4} - 1 \right] + \frac{1}{4} \left(\frac{\sigma_{22}}{F_{12}}\right)^2 + \left(\frac{\sigma_{23}}{F_{23}}\right)^2 + \frac{(\sigma_{12})^2 + (\sigma_{13})^2}{(F_{12})^2} \quad (1.3d)$$

The largest drawback of this theory is that there are two failure surfaces to check for each stress state.

The last failure criterion to be reviewed in this study is the maximum stress theory. Its form is,

$$F_{1c} < \sigma_{11} < F_{1t}$$

$$F_{2c} < \sigma_{22} < F_{2t}$$

$$|F_{12}| < \sigma_{12}$$

$$|F_{13}| < \sigma_{13}$$

$$|F_{23}| < \sigma_{23} \tag{1.4}$$

where F_{1c} , F_{1t} are the tensile and compressive strengths, respectively. The fact that the criterion is so widely used in industry justifies its adoption here.

Attention Patron:

Page 18 omitted from
numbering

where

- ${}^{L+\Delta L}\tau_{ij}$ = components of the Cauchy stress tensor
 ${}^{L+\Delta L}e_{ij}$ = components of the infinitesimal strain tensor going
 from configuration L to that of $L + \Delta L$
 f_i = components of the body force
 t_i = components of the applied tractions
 δu_i = components of the virtual displacements.

It is important to note that the Cauchy stress tensor is defined as the force divided by the area in the present configuration, whereas the 2nd Piola-Kirchhoff stress tensor is the force in the present configuration divided by the area in the original configuration:

$$\begin{array}{ll}
 \text{Cauchy Tensor} & \text{2nd Piola-Kirchhoff Tensor} \\
 \vec{dF} = (\underline{P} \cdot \hat{n})d^P A & \vec{dF} = (\underline{s} \cdot \hat{n})d^O A
 \end{array} \quad (2.5)$$

Since the total Lagrangian formulation uses the original configuration as the reference state, the 2nd Piola-Kirchhoff stress tensor is used rather than the Cauchy stress tensor. The relationship between the two is given by (see Malvern [68]),

$${}^{L+\Delta L}S_{ij} = \frac{{}^O\rho}{{}^{L+\Delta L}\rho} \frac{\partial {}^O x_i}{\partial {}^{L+\Delta L} x_m} {}^{L+\Delta L}\tau_{mn} \frac{\partial {}^O x_j}{\partial {}^{L+\Delta L} x_n} \quad (2.6)$$

where ${}^O\rho$, ${}^{L+\Delta L}\rho$ are the densities in the initial and future configurations respectively and the superscript o on ρ and x refers to the original configuration. The relationship between the infinitesimal strain tensor and the Green-Lagrange strain tensor is,

$${}^{L+\Delta L}e^{ij} = \frac{\partial {}^{L+\Delta L} x_k}{\partial {}^O x_i} \frac{\partial {}^{L+\Delta L} x_l}{\partial {}^O x_j} {}^{L+\Delta L}e_{kl} \quad (2.7)$$

Therefore, the left-hand side of the equilibrium equation becomes,

$$\int_{L+\Delta L_V}^{L+\Delta L} \tau_{ij} \delta({}^{L+\Delta L}e_{ij}) dV = \int_{o_V}^{L+\Delta L} {}_o S_{ij} \delta({}^{L+\Delta L}e_{ij}) dV \quad (2.8)$$

where ${}^{L+\Delta L}{}_o S_{ij}$ are the components of the 2nd Piola-Kirchhoff stress tensor corresponding to the configuration at $L + \Delta L$. The equilibrium equation now becomes,

$$\int_{o_V}^{L+\Delta L} {}_o S_{ij} \delta({}^{L+\Delta L}e_{ij}) dV = \int_{L+\Delta L_V}^{L+\Delta L} f_i \delta u_i dV + \int_{L+\Delta L_S}^{L+\Delta L} t_i \delta u_i dS \quad (2.9)$$

Energetically, the combination of the Cauchy stress tensor and the infinitesimal strain tensor is equivalent to that of the 2nd Piola-Kirchhoff stress tensor and the Green-Lagrange strain tensor. Following Bathe [66], incremental decompositions of the type,

$$\begin{aligned} {}^{L+\Delta L}{}_o S_{ij} &= {}^L{}_o S_{ij} + {}^o S_{ij} \\ {}^{L+\Delta L}{}_o e_{ij} &= {}^L{}_o e_{ij} + {}^o e_{ij} \end{aligned} \quad (2.10)$$

where the relations

$$\begin{aligned} {}^o e_{ij} &= {}^o e_{ij} + {}^o n_{ij} = \frac{1}{2} ({}_o u_{i,j} + {}_o u_{j,i} + {}^L u_{m,i} {}_o u_{m,j} + {}_o u_{m,i} {}^L u_{m,j}) \\ &\quad + \frac{1}{2} ({}_o u_{m,i} {}_o u_{m,j}) \\ {}^L{}_o e_{ij} &= \frac{1}{2} ({}^L u_{i,j} + {}^L u_{j,i} + {}^L u_{m,i} {}^L u_{m,j}) \\ {}^o S_{ij} &= C_{ijkl} {}^o e_{kl} \quad , \quad {}^L u_{i,j} = \frac{\partial {}^L u_i}{\partial {}^o x_j} \end{aligned} \quad (2.11)$$

are used.

Substituting the above relations into the equilibrium equation (2.8) results in the expression,

$$\int_{o_V} ({}^L S_{ij} + {}^o S_{ij}) \delta({}^o \epsilon_{ij}) dV = \int_{L+\Delta L_V}^{L+\Delta L} f_i \delta u_i dV + \int_{L+\Delta L_S}^{L+\Delta L} t_i \delta u_i dS$$

or, upon rearrangement,

$$\begin{aligned} \int_{o_V} C_{ijkl} o^{\epsilon_{kl}} \delta({}^o \epsilon_{ij}) dV + \int_{o_V} {}^L S_{ij} \delta({}^o \eta_{ij}) dV &= \int_{L+\Delta L_V}^{L+\Delta L} f_i \delta u_i dV \\ &+ \int_{L+\Delta L_S}^{L+\Delta L} t_i \delta u_i dS - \int_{o_V} {}^L S_{ij} \delta({}^o e_{ij}) dV \end{aligned} \quad (2.13)$$

At this point, linearization of the equilibrium equation is desirable in order to get a form suitable for finite element implementation. The assumptions made are,

$${}^o \epsilon_{ij} = o^e_{ij}$$

$${}^o S_{ij} = C_{ijkl} o^e_{kl}$$

Substituting these relations into Eq. (2.13), we obtain

$$\begin{aligned} &\int_{o_V} C_{ijkl} o^e_{kl} \delta({}^o e_{ij}) dV + \int_{o_V} {}^L S_{ij} \delta({}^o \eta_{ij}) dV \\ &= \int_{L+\Delta L_V}^{L+\Delta L} f_i \delta u_i dV + \int_{L+\Delta L_S}^{L+\Delta L} t_i \delta u_i dS - \int_{o_V} {}^L S_{ij} \delta({}^o e_{ij}) dV \end{aligned} \quad (2.14)$$

This is the form of the equilibrium equation which will be used to construct the 3-D degenerated shell element.

2.2 Finite Element Geometry and Formulation

The geometry of the element is presented here in detail following Zienkiewicz [69]. The coordinates of a typical point in the shell element (see Figure 2.1) are given by,

$$x_i = \sum_{j=1}^n \phi_j(\xi_1, \xi_2) \left[\frac{(1 + \xi_3)}{2} (x_j)_{i_{top}} + \frac{(1 - \xi_3)}{2} (x_j)_{i_{bottom}} \right] \quad (2.15)$$

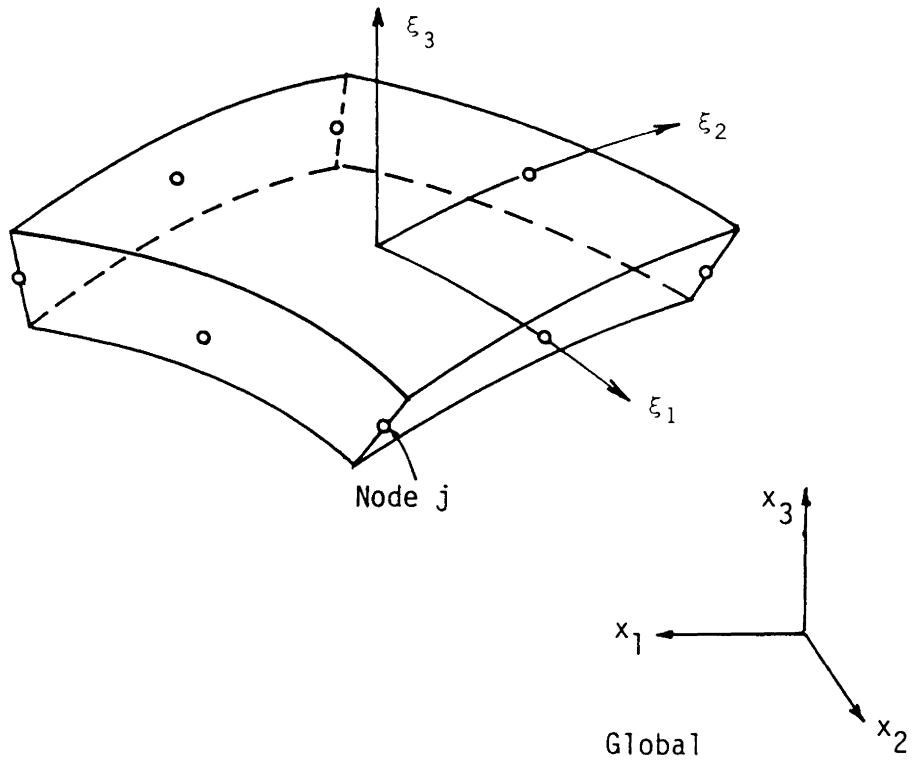


Figure 2.1 Local and global coordinate systems used in the 3-D degenerate shell finite element.

where

- ϕ_j = shape function associated with the element
- ξ_1, ξ_2, ξ_3 = normalized curvilinear coordinates
- $(x_j)_i$ = global coordinate in the i^{th} direction at node j
- n = number of nodes in the element

At node j , define a vector \vec{v}_3 such that,

$$\hat{e}_{3j} = \vec{v}_3 / |\vec{v}_3| \quad (2.16)$$

The components of \vec{v}_3 at node j in the i^{th} global direction are then (see Figure 2.2),

$$(\vec{v}_{3j})_i = (x_j)_{i_{\text{top}}} - (x_j)_{i_{\text{bottom}}} \quad (2.17)$$

Notice that the following relations also hold:

$$\begin{aligned} (x_j)_{i_{\text{mid}}} &= \frac{1}{2} [(x_j)_{i_{\text{top}}} - (x_j)_{i_{\text{bottom}}}] \\ \frac{\xi_3}{2} (v_{3j})_i &= \frac{\xi_3}{2} [(x_j)_{i_{\text{top}}} - (x_j)_{i_{\text{bottom}}}] \end{aligned} \quad (2.18)$$

Hence, a typical point in the element can now be described by the expression

$$x_i = \sum_{j=1}^n \phi_j(\xi_1, \xi_2) [(x_j)_{i_{\text{mid}}} + \frac{\xi_3}{2} (v_{3j})_i] \quad (2.19)$$

Denote the components of vector \hat{e}_3 at node j along the global x_i -axis as

$$(v_{3j})_i = h_j |\hat{e}_{3j}|_i \quad (2.20)$$

where h_j is the magnitude of \vec{v}_3 , or the thickness of the element at node j . The coordinates of a point in the element now become

$$x_i = \sum_{j=1}^n \phi_j(\xi_1, \xi_2) [(x_j)_{i_{\text{mid}}} + \frac{\xi_3 h_j}{2} |\hat{e}_{3j}|_i] \quad (2.21)$$

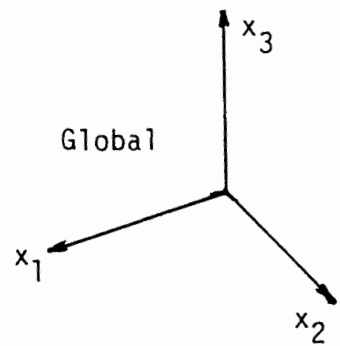
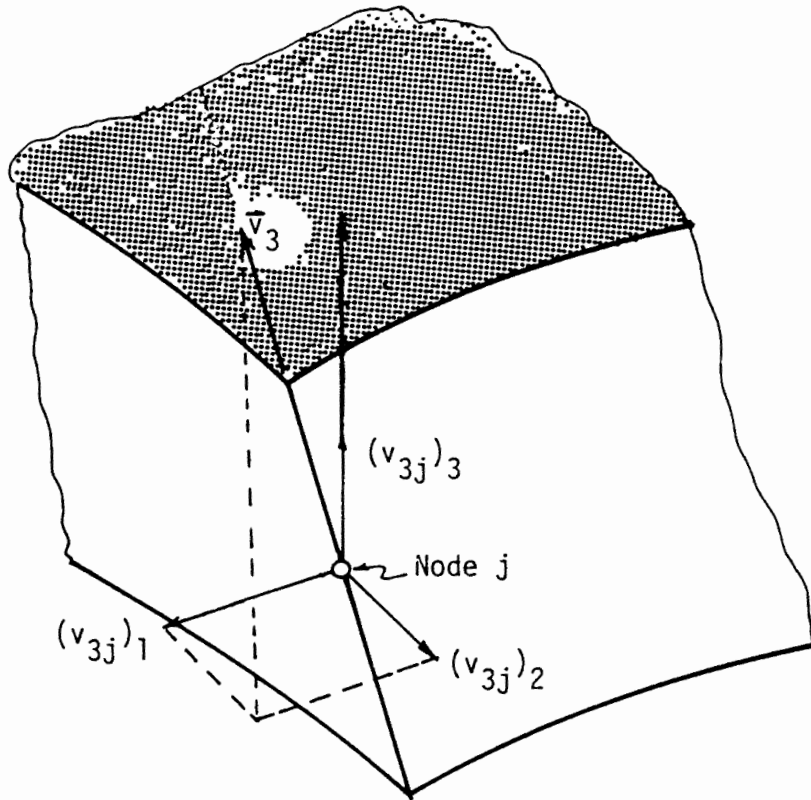


Figure 2.2 Vector \bar{v}_3 and its global components at node j.

Recall that,

$$\begin{aligned} L_{u_i} &= L_{x_i} - {}^0x_i \\ L+\Delta L_{u_i} &= L_{u_i} + {}^0u_i \end{aligned}$$

so that the displacements are approximated according to

$$L_{u_i} = \sum_{j=1}^n \phi_j(\xi_1, \xi_2) [(L_{u_j})_{i_{\text{mid}}} + \frac{\xi_3 h_j}{2} (|L\hat{e}_{3j}|_i - |{}^0\hat{e}_{3j}|_i)]. \quad (2.22)$$

The incremental displacements, given by

$$u_i = L+\Delta L_{u_i} - L_{u_i} \quad (2.23)$$

become

$$u_i = \sum_{j=1}^n \phi_j(\xi_1, \xi_2) [(u_j)_{i_{\text{mid}}} + \frac{\xi_3 h_j}{2} (|L+\Delta L\hat{e}_{3j}|_i - |L\hat{e}_{3j}|_i)]. \quad (2.24)$$

Define unit vectors $L\hat{e}_{1j}$ and $L\hat{e}_{2j}$ according to the relations

$$L\hat{e}_{1j} = \frac{\hat{E}_2 \times L\hat{e}_{3j}}{|\hat{E}_2 \times L\hat{e}_{3j}|} \quad \text{and} \quad L\hat{e}_{2j} = L\hat{e}_{3j} \times L\hat{e}_{1j} \quad (2.25)$$

where j is the node number, and \hat{E}_i are the global unit vectors in the i -th direction (see Figure 2.3). Assume that the rotations are small between load steps so that the incremental value of \hat{e}_{3j} at node j is,

$$\hat{e}_{3j} = \hat{e}_{1j}\theta_{2j} - \hat{e}_{2j}\theta_{1j} \quad (2.26)$$

where θ_{ij} is the rotation about local x_i -axis at node j . The components of \hat{e}_{3j} in the local system become

$$|\hat{e}_{3j}|_i = |L\hat{e}_{1j}|_i\theta_{2j} - |L\hat{e}_{2j}|_i\theta_{1j}. \quad (2.27)$$

The incremental value is given by

$$|L+\Delta L\hat{e}_{3j}|_i = |L\hat{e}_{3j}|_i + |{}^0\hat{e}_{3j}|_i. \quad (2.28)$$

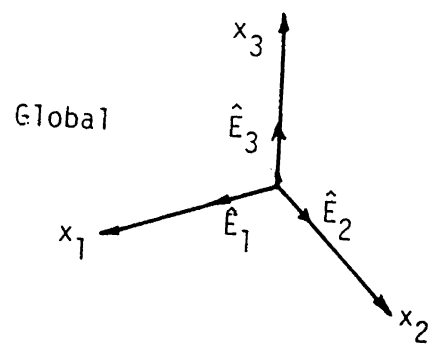
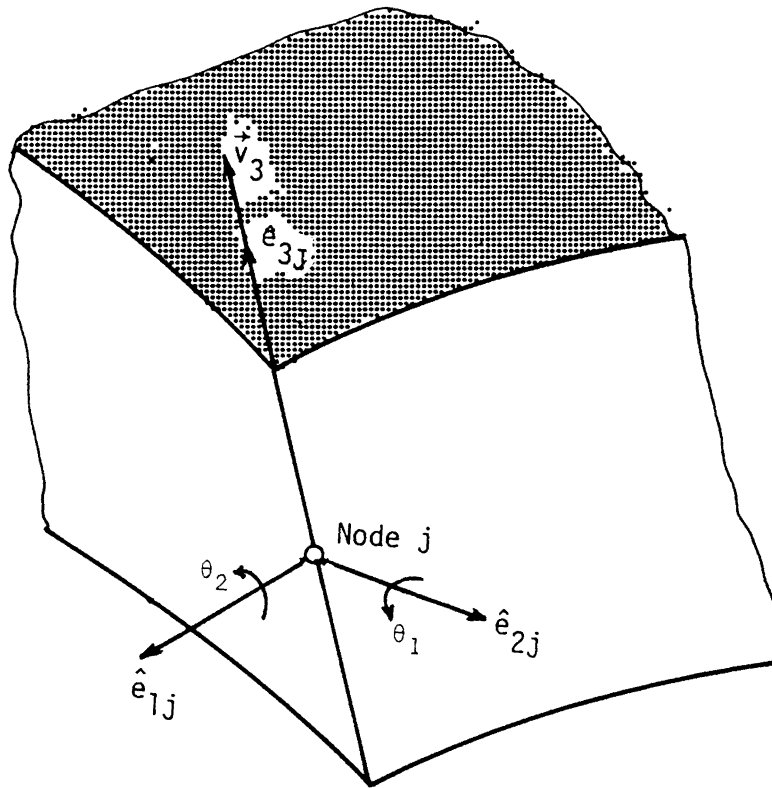


Figure 2.3 Element (local) and global unit vectors

Substituting Eq. (2.28) into Eq. (2.24), one obtains

$$u_i = \sum_{j=1}^n \phi_j(\varepsilon_1, \varepsilon_2) [(u_j)_{i_{\text{mid}}} + \frac{\varepsilon_3 h_j}{2} (|\hat{e}_{1j}|_{i_{\theta_{2j}}} - |\hat{e}_{2j}|_{i_{\theta_{1j}}})]. \quad (2.29)$$

Therefore, the displacements, in going from the configuration at L to that at $L + \Delta L$, are known when $(u_j)_{i_{\text{mid}}}$, θ_{1j} and θ_{2j} are known.

The development of the element equilibrium equations follows the work of Chao and Reddy [2]. The vector $\{u\}$ is defined as the column of displacements at a node in the element and is related to the midplane displacements and rotations, $\{\Delta\}$ according to

$$\begin{matrix} \{u\} \\ (3 \times 1) \end{matrix} = \begin{matrix} [T] \\ (3 \times 5n) \end{matrix} \begin{matrix} \{\Delta\} \\ (5n \times 1) \end{matrix} \quad (2.30)$$

where, $[T]$ is the transformation matrix defined by the incremental displacement equation and n is the number of nodes in the element. The strain-displacement equations for linear strain are

$$\{ {}_0 e \} = {}^L [A] \{ u_0 \} \quad (2.31)$$

where

$$\begin{aligned} \{ {}_0 e \} &= \{ {}_0 e_{11}, {}_0 e_{22}, {}_0 e_{33}, {}_2^0 e_{12}, {}_2^0 e_{13}, {}_2^0 e_{23} \}^T \\ \{ u_0 \} &= \{ {}_0^u u_{1,1}, {}_0^u u_{1,2}, {}_0^u u_{1,3}, {}_0^u u_{2,1}, {}_0^u u_{2,2}, {}_0^u u_{2,3}, {}_0^u u_{3,1}, {}_0^u u_{3,2}, {}_0^u u_{3,3} \}^T \end{aligned}$$

the derivatives are taken with respect to the original configuration,

and ${}^L [A]$ is the matrix relating e_{ij} to $u_{i,j}$:

$$\begin{aligned}
 L[A] = & \begin{bmatrix}
 1+L_{u_{1,1}} & 0 & 0 & L_{u_{2,1}} & 0 & 0 \\
 0 & L_{u_{1,2}} & 0 & 0 & 1+L_{u_{2,2}} & 0 \\
 0 & 0 & L_{u_{1,3}} & 0 & 0 & L_{u_{2,3}} \\
 L_{u_{1,2}} & 1+L_{u_{1,1}} & 0 & 1+L_{u_{2,2}} & L_{u_{2,1}} & 0 \\
 L_{u_{1,3}} & 0 & 1+L_{u_{1,1}} & L_{u_{2,3}} & 0 & L_{u_{2,1}} \\
 0 & L_{u_{1,3}} & L_{u_{1,2}} & 0 & L_{u_{2,3}} & 1+L_{u_{2,2}} \\
 \\
 L_{u_{3,1}} & 0 & 0 & \\
 0 & L_{u_{3,2}} & 0 & \\
 0 & 0 & 1+L_{u_{3,3}} & \\
 L_{u_{3,2}} & L_{u_{3,1}} & 0 & \\
 1+L_{u_{3,3}} & 0 & L_{u_{3,1}} & \\
 0 & 1+L_{u_{3,3}} & L_{u_{3,2}} &
 \end{bmatrix} \cdot \quad (2.32)
 \end{aligned}$$

The vectors, $\{_0u\}$ and $\{_0e\}$ are related to the displacement increments at the nodes by

$$\begin{aligned}
 \{_0u\} &= [N]\{u\} = [N][T]\{\Delta\} \\
 \{_0e\} &= L[A]\{_0u\} = L[A][N][T]\{\Delta\} \quad (2.33)
 \end{aligned}$$

where $[N]$ is

$$[N] = \begin{bmatrix} \frac{\partial}{\partial x_1} & 0 & 0 \\ \frac{\partial}{\partial x_2} & 0 & 0 \\ \frac{\partial}{\partial x_3} & 0 & 0 \\ 0 & \frac{\partial}{\partial x_1} & 0 \\ 0 & \frac{\partial}{\partial x_2} & 0 \\ 0 & \frac{\partial}{\partial x_3} & 0 \\ 0 & 0 & \frac{\partial}{\partial x_1} \\ 0 & 0 & \frac{\partial}{\partial x_2} \\ 0 & 0 & \frac{\partial}{\partial x_3} \end{bmatrix} . \quad (2.34)$$

Then the [B] matrix can now be formed as,

$$[B] = {}^L[A][N][T] \quad (2.35)$$

so that,

$$\{e\} = [B]\{\Delta\}. \quad (2.36)$$

Using the definition of the [B] matrix and substituting it into Eq. (2.13), one obtains

$$({}^L[K_L] + {}^L[K_{NL}])\{\Delta\} = {}^{L+\Delta L}\{R\} - {}^{L+\Delta L}\{F\} \quad (2.37)$$

where ${}^L[K_L]$, ${}^L[K_{NL}]$, ${}^{L+\Delta L}\{R\}$, ${}^{L+\Delta L}\{F\}$ are the linear and non-linear stiffness matrices, the external force vector, and the unbalanced force vector, respectively. Explicitly,

$$\begin{aligned}
{}^L[K_L] &= \int_{o_V} [B]^T [C] {}^L[B] dV \\
{}^L[K_{NL}] &= \int_{o_V} [B]^T [S] [B] dV \\
{}^{L+\Delta L}\{F\} &= \int_{o_V} [B]^T \{\hat{S}\} dV
\end{aligned} \tag{2.38}$$

where $[S]$ and $\{\hat{S}\}$ are the matrix and vector forms of the 2nd Piola-Kirchhoff stress tensor.

2.3 Material Nonlinearity

The inclusion of material nonlinearity into the analysis becomes essential to accurately predict stress states well above yield stress levels. In this study, the material nonlinearity will be modelled by using the associated flow rule with isotropic work hardening. The associated flow rule states that the plastic strain is related to the stress in the following manner:

$$\{d\epsilon\}_{pl} = \lambda \left\{ \frac{dF}{d\sigma} \right\} \tag{2.39}$$

where λ is a constant, and

$\{d\epsilon\}_{pl}$ = incremental plastic strain components

F = yield function (modified Von Mises)

$\{\sigma\}$ = vector of the components of stress.

Recalling that elastic strains can be found from the derivative of the elastic strain energy density function with respect to the appropriate stress components, it is seen that the associated flow rule will yield plastic strain increments in a similar manner where the yield function serves as a plastic potential.

The constant is evaluated by requiring that during plastic deformation, the stress state remains on the boundary of the yield function. Therefore,

$$dF = \left\{ \frac{\partial F}{\partial \sigma} \right\} \{d\sigma\} - H\lambda = 0$$

$$\frac{\partial F}{\partial \sigma_{11}} d\sigma_{11} + \frac{\partial F}{\partial \sigma_{22}} d\sigma_{22} + \frac{\partial F}{\partial \sigma_{12}} d\sigma_{12} + \frac{\partial F}{\partial \sigma_{13}} d\sigma_{13} + \frac{\partial F}{\partial \sigma_{23}} d\sigma_{23} - H\lambda = 0$$

or,

$$\left\{ \frac{\partial F}{\partial \sigma} \right\}^T \{d\sigma\} - H\lambda = 0. \quad (2.40)$$

Recall the elastic strain increment is related to the stress increment by Hooke's law as

$$\{d\epsilon\}_{\text{elastic}} = \{d\sigma\}/[E]$$

where $[E]$ is the elastic stiffness matrix. The total strain is

$$\{d\epsilon\}_{\text{total}} = \{d\epsilon\}_{\text{elastic}} + \{d\epsilon\}_{\text{plastic}}$$

therefore, the stresses in terms of the total and plastic strains become

$$\{d\sigma\} = [E](\{d\epsilon\}_{\text{total}} - \{d\epsilon\}_{\text{plastic}}).$$

The constant can now be evaluated from the associated flow rule as,

$$\left\{ \frac{\partial F}{\partial \sigma} \right\}^T [[E](\{d\epsilon\}_{\text{total}} - \lambda \left\{ \frac{\partial F}{\partial \sigma} \right\})] - H\lambda = 0, \quad (2.41)$$

where H is the slope of the effective stress vs. effective strain curve in the reference direction for the material, and the constant is the incremental effective plastic strain. The constitutive relation then becomes

$$\{d\sigma\} = [E](\{d\epsilon\}_{\text{total}} - \frac{\left\{ \frac{\partial F}{\partial \sigma} \right\} \left\{ \frac{\partial F}{\partial \sigma} \right\}^T [E] \{d\epsilon\}_{\text{total}}}{H + \left\{ \frac{\partial F}{\partial \sigma} \right\}^T [E] \left\{ \frac{\partial F}{\partial \sigma} \right\}}) \quad (2.42)$$

or,

$$\{d\sigma\} = [E^{ep}]\{d\varepsilon\}_{total}$$

where

$$[E^{ep}] = [E] - \frac{[E]\left\{\frac{\partial F}{\partial \sigma}\right\}\left\{\frac{\partial F}{\partial \sigma}\right\}^T [E]}{H + \left\{\frac{\partial F}{\partial \sigma}\right\}^T [E]\left\{\frac{\partial F}{\partial \sigma}\right\}}. \quad (2.43)$$

Hence, for plastically behaving Gauss points, the second term on the right hand side is evaluated, and for elastically behaving Gauss points, this term is set to zero.

The plasticity function used in this study is the modified Von Mises yield criterion in the form used by Chandrashekhara and Reddy [3],

$$(\bar{\sigma}_0)^2 = B_1\sigma_1^2 - B_2\sigma_1\sigma_2 + B_3\sigma_2^2 + 3B_6\sigma_{23}^2 + 3B_5\sigma_{13}^2 + 3B_4\sigma_{12}^2 \quad (2.44)$$

where

$\bar{\sigma}_0$ = effective stress

B_i = independent parameters of anisotropy.

The B_i are the parameters that will be updated when the material becomes plastic. Using the fiber direction (the x_1 -direction) of the lamina as reference, the B_i in the elastic region are

$$\begin{aligned} B_1 &= \frac{\sigma_0^2}{\sigma_{01}^2} = 1.0 & B_6 &= \frac{1}{3} \frac{\sigma_0^2}{\sigma_{023}^2} & B_4 &= \frac{1}{3} \frac{\sigma_0^2}{\sigma_{012}^2} \\ B_3 &= \frac{\sigma_0^2}{\sigma_{02}^2} & B_5 &= \frac{1}{3} \frac{\sigma_0^2}{\sigma_{013}^2} \end{aligned} \quad (2.45)$$

where σ_{0ij} are the initial yield stresses. To obtain B_2 , a tensile test in the plane of the lamina on a specimen cut at 45° to the fiber direction is to be used. The stresses are,

$$\begin{aligned}\sigma_1 = \sigma_2 = \sigma_{12} &= \frac{1}{2} \sigma_{045} \\ \sigma_{23} = \sigma_{13} &= 0\end{aligned}\quad (2.46)$$

where σ_{045} is the initial yield strength of the lamina in the 45° direction. Therefore,

$$\frac{-2}{\sigma_0} = \sigma_{045}^2 \left[\frac{1}{4} - B_2 \frac{1}{4} + B_3 \frac{1}{4} + 3B_4 \frac{1}{4} \right]$$

or,

$$B_2 = 1 + \frac{\frac{-2}{\sigma_0}}{\sigma_{02}^2} + \frac{\frac{-2}{\sigma_0}}{\sigma_{012}^2} - 4 \frac{\frac{-2}{\sigma_0}}{\sigma_{045}^2}\quad (2.47)$$

The plastic anisotropic parameters are found using the work hardening rule which states that the plastic work done by each stress component will be the same. Let,

σ_1^H = uniaxial yield stress in the x_1 direction including hardening effects

$\bar{\sigma}$ = corresponding effective stress

ϵ_1^P = plastic strain in the x_1 direction

E_{p1} = slope of the stress vs. plastic-strain curve in the x_1 direction

For σ_1^H and σ_2^H to correspond to the same effective stress, $\bar{\sigma}$, the work done should be the same. Therefore, from Figure 2.4a, one obtains,

$$\sigma_{01} \epsilon_1^P + \frac{1}{2} \epsilon_1^P (\sigma_1^H - \sigma_{01}) = \sigma_{02} \epsilon_2^P + \frac{1}{2} \epsilon_2^P (\sigma_2^H - \sigma_{02}).\quad (2.48)$$

Note that,

$$\epsilon_1^P = (\sigma_1^H - \sigma_{01})/E_{p1}$$

$$\epsilon_2^P = (\sigma_2^H - \sigma_{02})/E_{p2}.$$

Therefore,

$$\frac{\sigma_{01}}{E_{p1}} (\sigma_1^H - \sigma_{01}) + \frac{(\sigma_1^H - \sigma_{01})^2}{2E_{p1}} = \frac{\sigma_{02}}{E_{p2}} (\sigma_2^H - \sigma_{02}) + \frac{(\sigma_2^H - \sigma_{02})^2}{2E_{p2}}$$

or

$$\frac{(\sigma_1^H)^2 - (\sigma_{01})^2}{2E_{p1}} = \frac{(\sigma_2^H)^2 - (\sigma_{02})^2}{2E_{p2}}$$

so,

$$(\sigma_2^H)^2 = \frac{E_{p2}}{E_{p1}} [(\sigma_1^H)^2 - (\sigma_{01})^2] + (\sigma_{02})^2. \quad (2.49)$$

Since the reference direction is the x_1 -direction, $B_1 = 1.0$, and therefore $\bar{\sigma} = \sigma_1^H$. Hence,

$$(\sigma_2^H)^2 = \frac{E_{p2}}{E_{p1}} [(\bar{\sigma})^2 - (\sigma_{01})^2] + (\sigma_{02})^2$$

so the plastic B_3 is

$$B_3 = \frac{\frac{-2}{\bar{\sigma}}}{(\sigma_2^H)^2} = \frac{\frac{-2}{\bar{\sigma}}}{\frac{E_{p2}}{E_{p1}} [(\bar{\sigma})^2 - (\sigma_{01})^2] + (\sigma_{02})^2}. \quad (2.50)$$

Similarly, using Figure 2.4b,

$$B_6 = \frac{\frac{-2}{\bar{\sigma}}}{3(\sigma_{23}^H)^2} = \frac{\frac{-2}{\bar{\sigma}}}{3[\frac{G_{p23}}{E_{p1}} (\bar{\sigma}^2 - \sigma_{01}^2) + (\sigma_{023})^2]} \quad (2.51)$$

$$B_5 = \frac{\frac{-2}{\bar{\sigma}}}{3(\sigma_{13}^H)^2} = \frac{\frac{-2}{\bar{\sigma}}}{3[\frac{G_{p13}}{E_{p1}} (\bar{\sigma}^2 - \sigma_{01}^2) + (\sigma_{013})^2]} \quad (2.52)$$

$$B_4 = \frac{\frac{-2}{\bar{\sigma}}}{3(\sigma_{12}^H)^2} = \frac{\frac{-2}{\bar{\sigma}}}{3[\frac{G_{p12}}{E_{p1}} (\bar{\sigma}^2 - \sigma_{01}^2) + (\sigma_{012})^2]} \quad (2.53)$$

For B_2 , use Figure 2.4c and recall that elastically

$$B_2 = 1 + B_3 + B_4 - 4 \frac{\sigma_0^2}{(\sigma_{045}^H)^2}$$

where σ_{045}^H becomes

$$(\sigma_{045}^H)^2 = \frac{E_{P45}}{E_{P1}} (\sigma^2 - \sigma_{01}^2) + (\sigma_{045})^2 \quad (2.54)$$

Therefore, we have

$$B_2 = 1 + B_3 + B_4 - \frac{4\sigma^2}{\frac{E_{P45}}{E_{P1}} (\sigma^2 - \sigma_{01}^2) + (\sigma_{045})^2}. \quad (2.55)$$

The independent anisotropic parameters vary as a function of plastic strain (they do not change if no plastic strain occurs). In general, the stresses will be calculated in the material principal axes system, so that the stresses must be transformed from the global axes as follows:

$$\sigma_1 = \sigma_x \cos^2 \theta + \sigma_y \sin^2 \theta + 2\sigma_{xy} \sin \theta \cos \theta$$

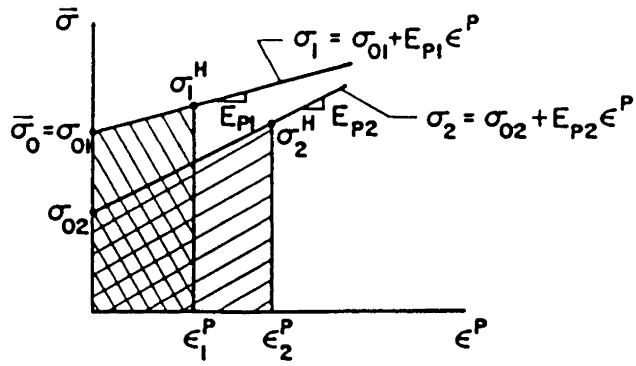
$$\sigma_2 = \sigma_x \sin^2 \theta + \sigma_y \cos^2 \theta - 2\sigma_{xy} \sin \theta \cos \theta$$

$$\sigma_{23} = -\sigma_{xz} \sin \theta + \sigma_{yz} \cos \theta$$

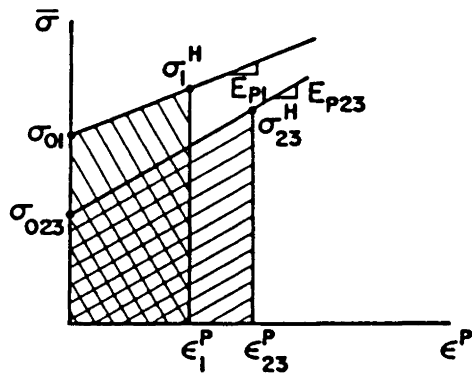
$$\sigma_{13} = \sigma_{xz} \cos \theta + \sigma_{yz} \sin \theta$$

$$\sigma_{12} = -\sigma_x \sin \theta \cos \theta + \sigma_y \sin \theta \cos \theta + \sigma_{xy} (\cos^2 \theta - \sin^2 \theta). \quad (2.56)$$

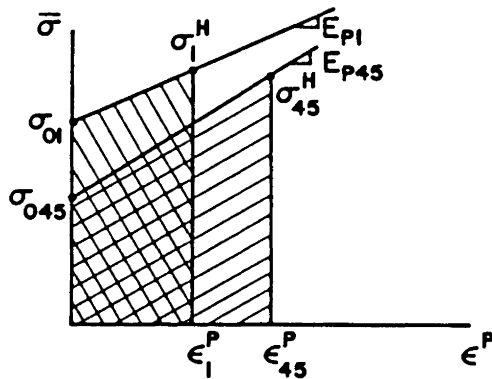
As mentioned earlier, the stress state must remain on the boundary of the plasticity function in order to evaluate the plastic strains.



(a)



(b)



(c)

Figure 2.4 Effective plastic stress-strain relations

The scheme to reduce the stresses to the boundary at each load step in the program will be the one used by Chandrashekhara and Reddy [3].

2.4 Computational Procedure

The total load is divided into a number of load steps. At each load step, the global stiffness matrices and force vectors are assembled, boundary conditions are applied, and the solution vector is calculated (see [70]). If the displacement solution is not within a specified amount of error, an iteration process at this load step begins using the full Newton-Raphson technique. Once the displacement solution is obtained at this load level, the stresses and strains are calculated at the top and bottom of each lamina at the Gauss points of the element. Then the material nonlinearity is checked in each element at each Gauss point. If no Gauss points of an element pass the criterion, the element stiffnesses are reduced. After all elements are checked, the load step is increased, and the process is repeated. A flow chart of the general procedure is shown in Figure 2.5.

If, after the geometric nonlinearity has converged, it is found that a Gauss point is not elastic, a re-estimation of the stiffnesses to get this Gauss point's stress state on the yield function surface is done. The same load step is rerun until all of the Gauss point stress state are at least on the surface of their respective yield functions. The failure criterion is then checked.

When the failure criterion is violated, the failed constitutive matrix at that Gauss point, of that lamina, in that element is set nearly to zero. This is to reflect the fact that for at least some

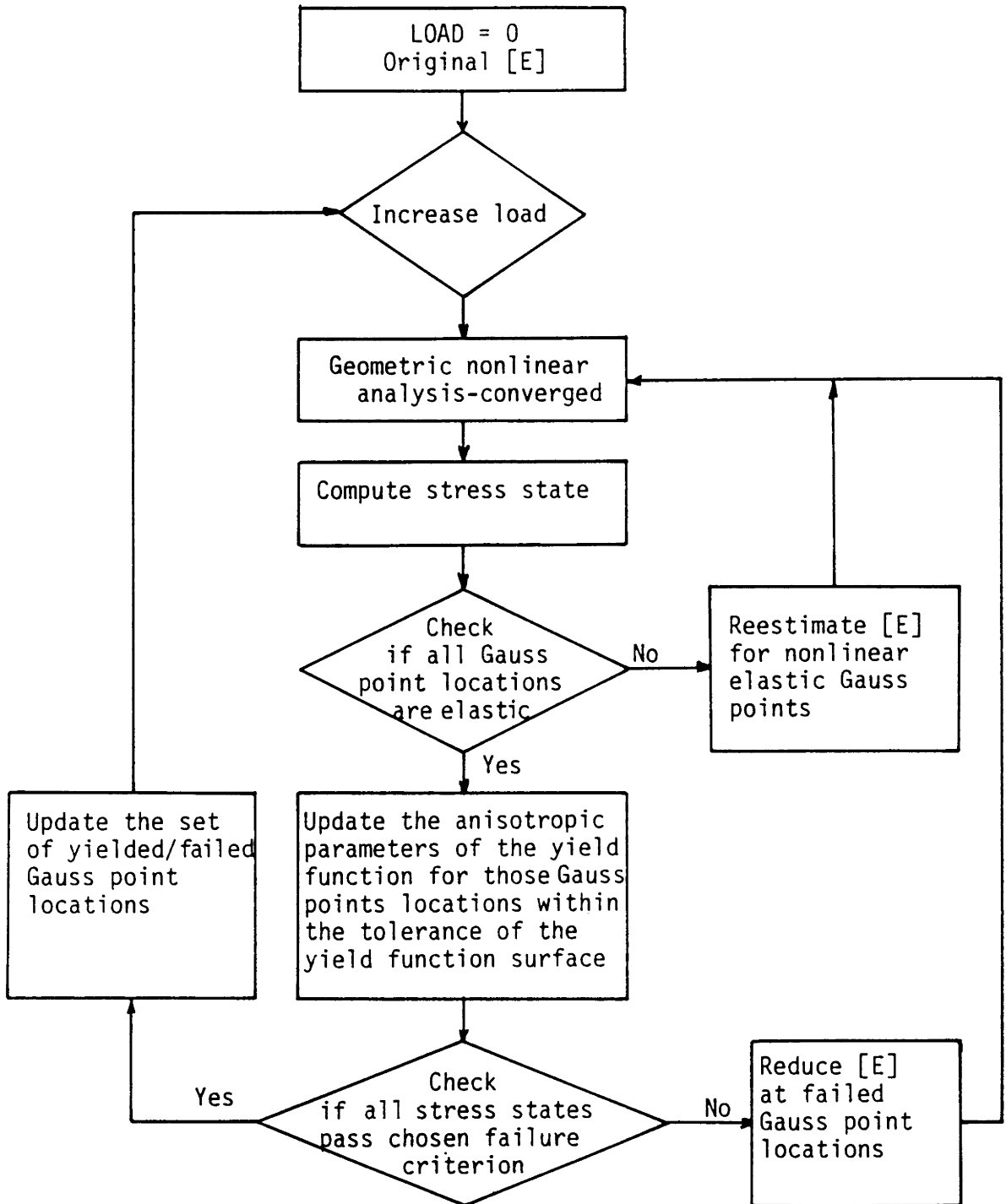


Figure 2.5 A computer flow chart of the finite element procedure for elastic-plastic and failure analysis.

distance, this portion of the structure will be ineffective in carrying load. Due to shear transfer within the laminate, the load will be rerouted around the failed area. This idea is similar to the one employed in micromechanical arguments about how load is transferred in the matrix around a cracked fiber.

The manner in which the material stiffness matrix is reduced when its corresponding stress state violates the failure criterion varies with the failure criterion. For the Tsai-Wu, Mathers-Hill, and maximum stress theories, each element in the 5×5 material stiffness matrix is set equal to unity. There is no allowance made for prediction of the mode of failure for any of these three theories, therefore a failure is interpreted as a non-load carrying condition at that point in the structure.

If failure is predicted by Hashin's mode theory either the first row and first column, or the intersection of the bottom four rows and right-most four columns of the failed constitutive matrix are set to unity when a fiber or matrix failure, respectively, is predicted. If any Gauss points have violated the failure criterion, the entire load step must be rerun. Only after all Gauss points pass this section is the load increased.

As the load increases, a section of the structure will become very weak due to the reduced stiffness at the Gauss points. After a specified reduction of strength, the structure is considered to have failed, and the program ends.

Note that the full (rather than modified) Newton-Raphson iteration technique is used in this program. As pointed out by Bahei-El-Din [28],

Attention Patron:

Page 40 omitted from
numbering

Third, the stress states are computed on the 2x2 Gauss point grid within each element since full, 3x3 Gauss quadrature is used to compute the displacement solution.

Fourth, there are two material stiffness matrices at each Gauss point location in each lamina in each element. Therefore, there are a total of $[(NOE - 1)*NOL*13 + (NOL - 1)*13 + 13]$ constitutive matrices per model.[‡] These matrices are the ones being manipulated by the plasticity and failure theory subroutines.

Fifth, since there is, in general, a variation of material properties through the thickness of each lamina in an element, the integration in this direction must be modified. The integration through the thickness is now carried out over half of each lamina using the appropriate material stiffness matrix. For example, to integrate through the thickness of a laminate composed of N layers, the integral

$$\int_{\eta} \int_{\xi} \int_{\zeta} [B]^T [\bar{Q}] [B] d\zeta d\xi d\eta$$

where [B] is in general a function of ζ becomes

$$\int_{\eta} \int_{\xi} \sum_{k=1}^{2N} \int_{\zeta_k}^{\zeta_{k+1}} f(\zeta^N) [\bar{Q}]_k d\zeta d\xi d\eta \quad (2.57)$$

where N is the total number of layers and $n = 0,1,2$ in this study. Note that there are two layers within each lamina, each having its own material stiffness matrix. This allows the upper portion of a lamina to act independently of the lower portion in the sense that the upper portion may go plastic, while the lower one remains elastic. This

[‡]where NOE = number of elements in the model
 NOL = number of layers in the model

approach is adopted because, in general, the stress states are most severe at the top and bottom of each lamina.

2.6 Reducing Stress States to the Plasticity Function Surface

From the material nonlinear description one can define

$$[W] \equiv \frac{\left\{ \frac{\partial F}{\partial \sigma} \right\}^T [E]}{H + \left\{ \frac{\partial F}{\partial \sigma} \right\}^T [E] \left\{ \frac{\partial F}{\partial \sigma} \right\}} \quad (2.58)$$

so that the incremental effective plastic strain is

$$d\varepsilon^P = [W]d\varepsilon$$

and Hookes law generalized to the plastic region becomes

$$\{d\sigma\} = ([E] - [E] \left\{ \frac{\partial F}{\partial \sigma} \right\} [W]) \{d\varepsilon\}$$

or,

$$\{d\sigma\} = [E^{ep}] \{d\varepsilon\}. \quad (2.59)$$

The technique to satisfy plasticity is to:

- 1) choose an $[E^{ep}]$
- 2) compute displacements
- 3) compute the total and plastic strains
- 4) compute stresses
- 5) check to see that stress states satisfy the plasticity function
 - If not: a) reestimate $[E]$ of the Gauss points that failed
 - b) repeat 2) through 5) until stresses are converged.

Now the $[E^{ep}]$ at hand satisfies the plasticity surface requirement and stress-strain relations in elastic and plastic regions. When using linear strains, one can get the stress states back down to the plasticity function surface by setting up a scalar factor

$$x_m = 1 - \frac{\bar{\sigma}_0}{\bar{\sigma}_{\text{computed}}} \quad (2.60)$$

For the incremental effective plastic strain,

$$d\bar{\epsilon}^P = [W] \{d\epsilon\} (x_m)$$

where $\{d\epsilon\} (x_m)$ is the elastic portion of the total strain and the modified Hooke's law is

$$\{d\sigma\} = ([E] - (x_m)[E] \left\{ \frac{\partial F}{\partial \sigma} \right\} [W]) \{d\epsilon\} \quad (2.61)$$

where

$$[E^{\text{ep}}] = ([E] - (x_m)[E] \left\{ \frac{\partial F}{\partial \sigma} \right\} [W]). \quad (2.62)$$

Notice the role of x_m ; it tells one how much of the strain is elastic and how much is plastic. This is necessary to know when computing the effective plastic strain increment, and eventually, the individual plastic strain increments. It is not necessary to know how much of the total strain is elastic or plastic when computing the incremental stresses. However, when linear strains are used, it is convenient to use x_m as shown above.

When nonlinear strains are used, there is no guarantee that the use of x_m will lead to convergence. The displacements, computed using the reduced stiffnesses, may cause strains that are high enough to produce an increased stress state. One expects greater displacements and strains due to the decreased stiffnesses, but one also expects decreased stress states for the same reason. The use of x_m with linear strains gives the expected results; with nonlinear strains, in general, it fails, or requires smaller load steps, for the continuum based element.

Attention Patron:

Page 44 omitted from
numbering

Attention Patron:

Page 45 omitted from
numbering

CHAPTER 3

NUMERICAL RESULTS

Several example problems are discussed to illustrate the capabilities of the 3-D degenerated shell element developed here. All examples discussed here the nine-node quadratic element is used [70]. All of the computations were carried out on an IBM 3090 in double precision arithmetic. The examples in Sections 3.1-3.5 are used to evaluate the accuracy of the element, and the remaining examples are presented to investigate the effects of shear deformation, anisotropy and plastic deformation on the solutions. Note that the present element is quite general. It can model arbitrary geometries, including beams, plates, cylindrical shell panels and spherical shell panels as special cases. While the geometries considered in the present study fall into the special cases, the generality of the element permits one to analyze more complex structures, provided a preprocessor can be developed to input such geometries to the present program. Another important feature of the present element is that the geometry is updated during the loading (see Ref. [67]) in contrast to elements based on plate and shell theories (see Ref. [3]).

3.1 Isotropic Thick Plate

Figure 3.1 shows the load versus deflection curve of a clamped isotropic thick plate under uniform pressure loading. The formulation accounts for the geometric changes, and therefore the pressure load always acts normal to the surface during deformation. The geometry and boundary conditions used are also shown in Fig. 3.1. Material type 5

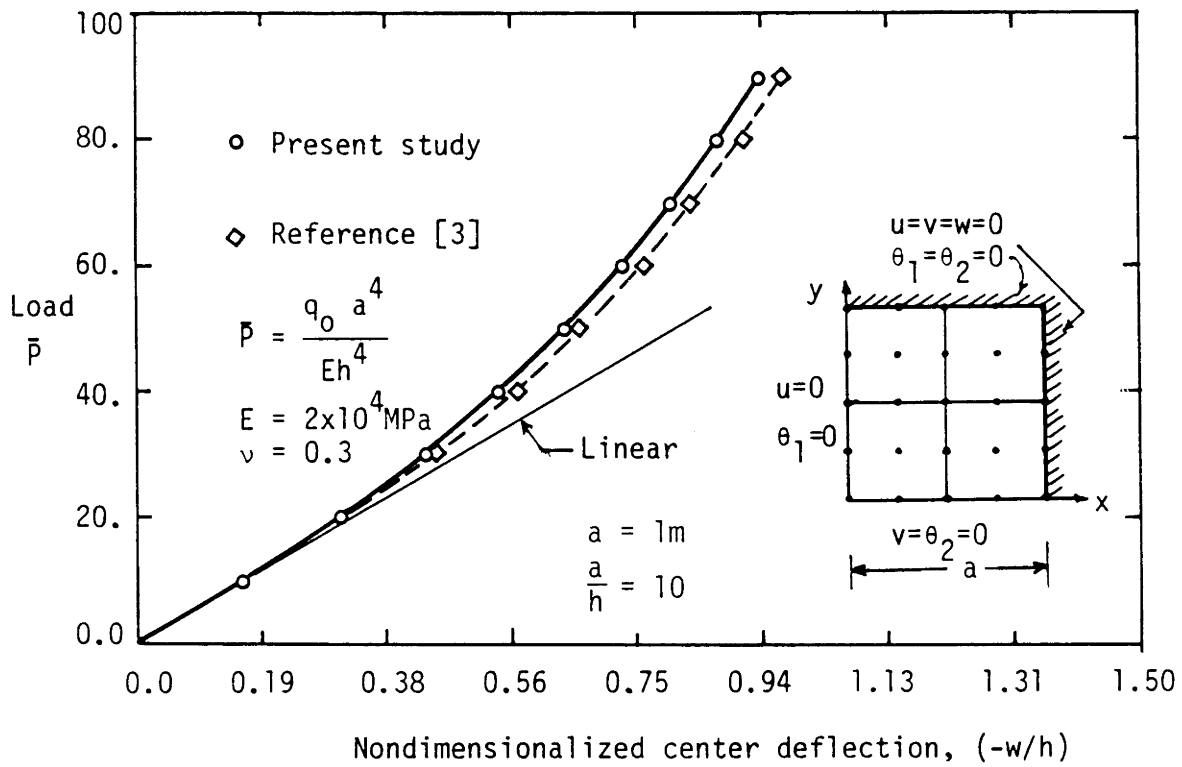


Figure 3.1 Bending of a clamped square plate (isotropic) under uniform transverse load of intensity q_0 ($a/h=10$).

(see Appendix) is used. The side length to thickness ratio is ten. Good correlation with the results of reference [3] is observed.

3.2 Orthotropic and Cross-Ply Thin Plates

Clamped orthotropic and cross-ply square plates under uniform pressure load are analyzed, and the load versus deflection curves are compared in Figure 3.2 with the results from reference [3], which is based on a shell theory. The plate has a side length to thickness ratio of 500, and made of material type 4. Notice that both plates have large geometric nonlinear effects even when centerline deflections are only one and a half times the plate thickness. The difference between the present solution and that of Ref. [3] is possibly due to the fact that the present formulation accounts for geometric changes during deformation.

3.3 Isotropic Cylindrical Shell Panel

Figure 3.3 shows the load versus centerline deflection of a clamped, thin cylindrical shell panel of material type 6 under a uniform pressure load. The present results show a greater "softening" than that in Ref. [3]. Again, this is due to the fact that the present element accounts for geometric changes during loading. Good agreement is observed, as both show an eventual stiffening of the panel.

3.4 Isotropic Spherical Shell Panel

A square edged isotropic spherical shell panel, or an end cap, is analyzed and the results are compared to the results of a circular-edged shell (see [60]) of material type 3 with clamped boundary conditions in

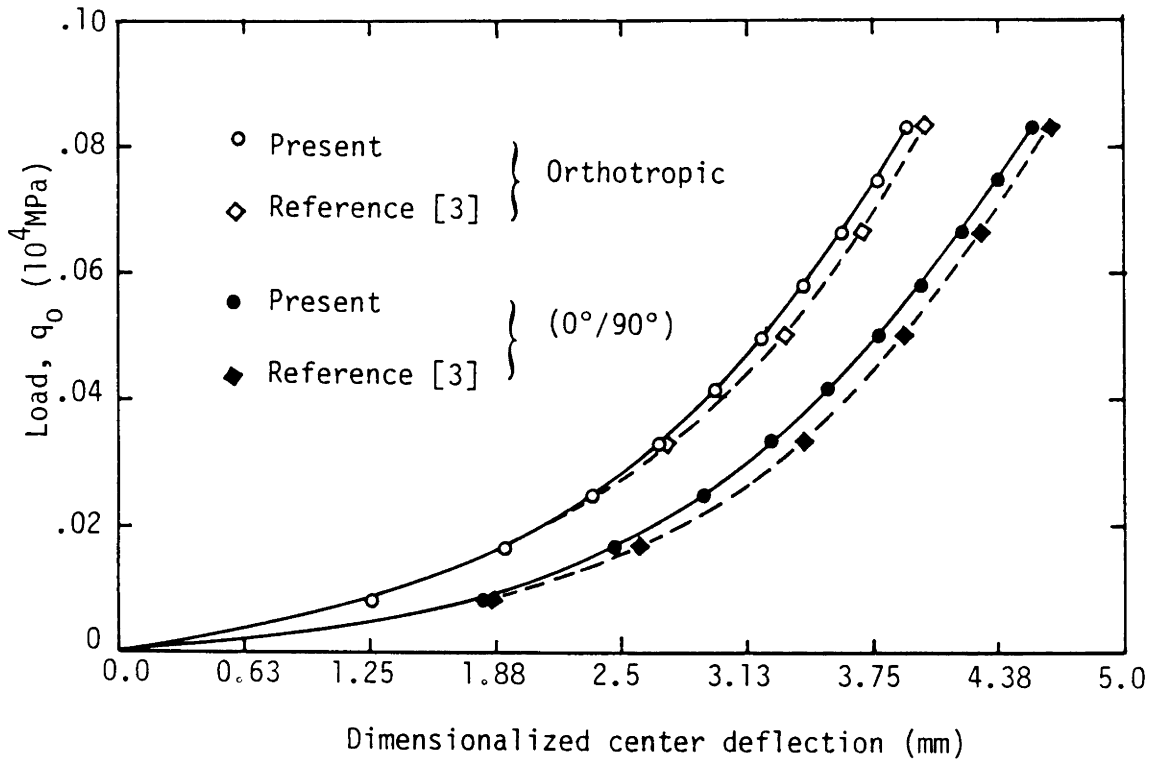


Figure 3.2 Bending of orthotropic and cross-ply ($0^\circ/90^\circ$), clamped square laminates under uniform distributed transverse load (q_0) [$a=1,000$ mm, $h=2$ mm, $E_1=12.5E_2$, $E_2=2 \times 10^4$ N/mm², $G_{12}=G_{23} \stackrel{9}{=} 10^4$ N/mm², $G_{23}=0.4 \times 10^4$ N/mm², $\nu_{12}=0.275$]

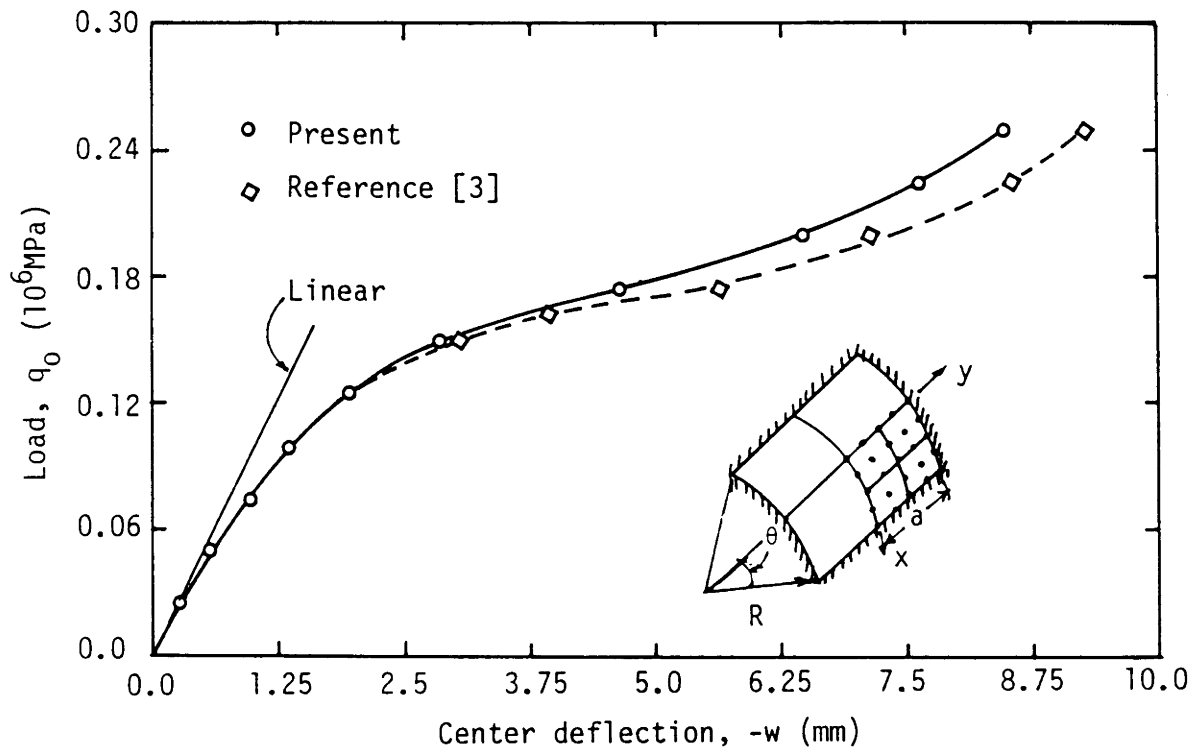


Figure 3.3 Bending of a thin, isotropic, clamped cylindrical shell under uniform pressure load [$E=3103$ N/mm², $\nu=0.3$, $a=254$ mm, $R=10a$, $h=3.175$ mm, $\theta=0.1$ rad]

Figure 3.4. The circular shell cap fits inside the square shell panel, and thus one expects a stiffer response from the square shell panel. Both spherical shells undergo twelve load steps of 80 psi. The response of each shell is similar, with the circular shell of Ref. [60] being "softer" as expected. Both shells show the hardening effect after an initial softening effect.

3.5 Combined Nonlinear Effects on thin Cylindrical Shells

An isotropic, clamped, thin ($a/h = 160$) cylindrical shell panel under uniform pressure loading is analyzed to determine the effect of the material nonlinearity on the deflection. Material type 7 is used (low yield stress, perfectly plastic behavior).

Figure 3.5 contains the plots of the load versus centerline deflection for linear, geometric nonlinear, and combined geometric and material nonlinear cases. Note that the shell panel exhibits the same general behavior as was previously shown in Figure 3.3; an initial softening followed by stiffening of the structure. The material nonlinearity does not affect the solution appreciably until the stiffening action occurs. When stiffening does occur, the cylindrical shell behaves in a similar fashion to a flat plate; the material nonlinearity softens the shell panel while the geometric nonlinearity stiffens the shell.

Results of the combined nonlinearity on a cross-ply, thin, shallow shell panel are presented in Figure 3.6. The shell panel is made of material type 2. The edges are clamped and a uniform pressure load is applied. The side length-to-thickness ratio is 32. Note that the

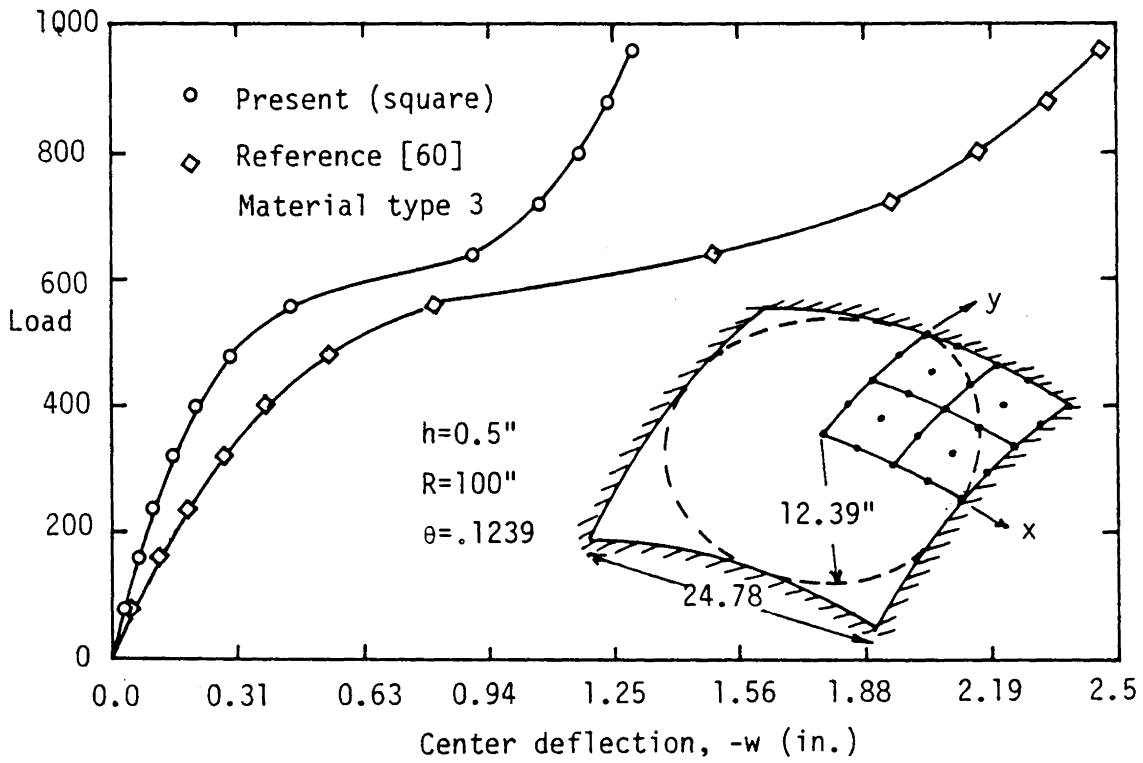


Figure 3.4 Bending of clamped, isotropic, spherical shell panels under uniform load

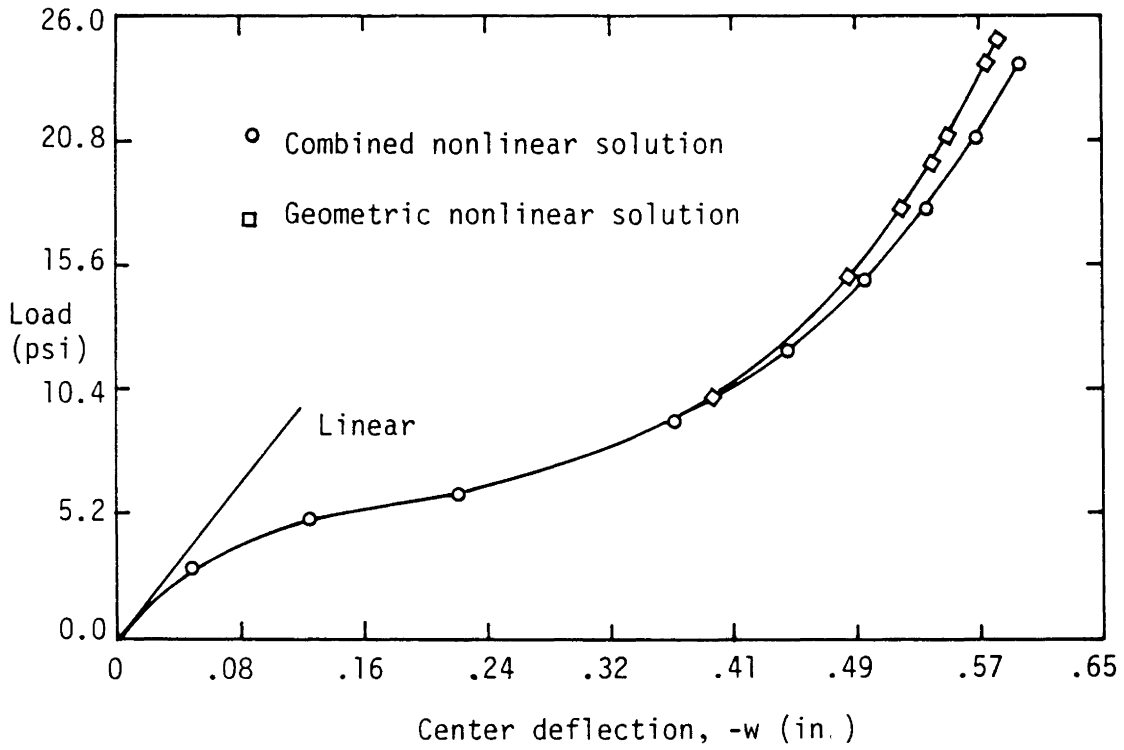


Figure 3.5 Bending of a thin, isotropic cylindrical shell panel under pressure load.

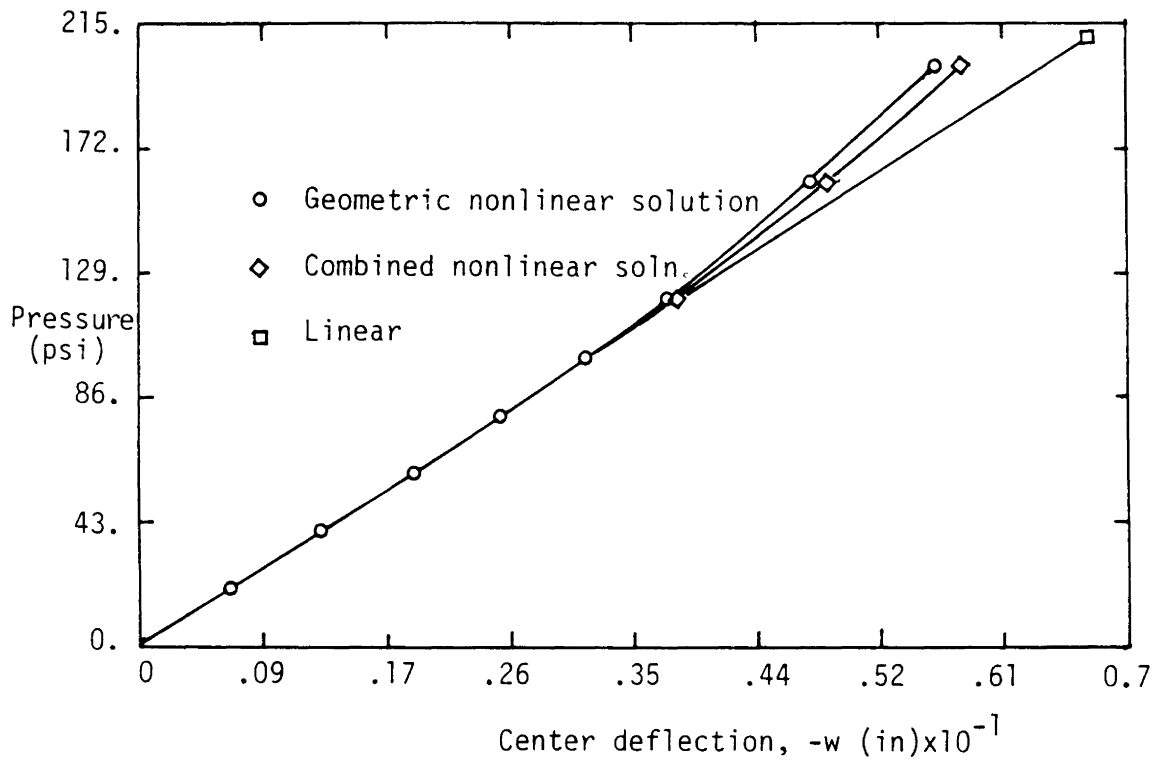


Figure 3.6 Bending of a shallow, thin, cross-ply ($0^{\circ}/90^{\circ}$) cylindrical shell panel under pressure loading.

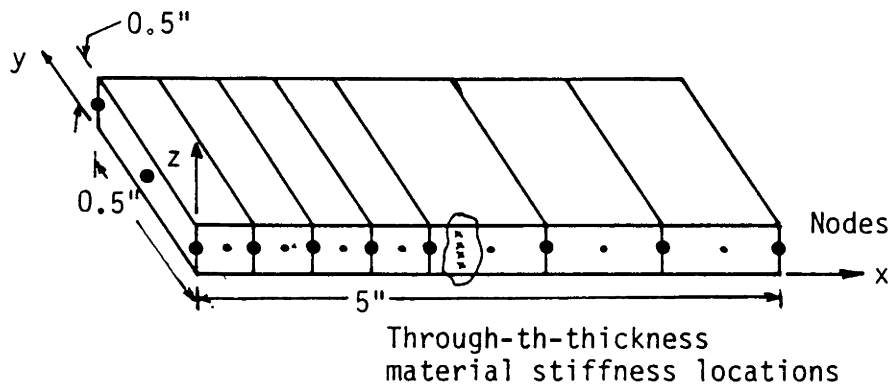
shallow shell panel exhibits entirely different behavior than the isotropic shell panel discussed in the preceding paragraphs. The behavior is very much like that of a flat plate, with the geometric nonlinear effect dominating the material nonlinear effect through the entire load range considered here. From the results, it is noted that the matrix in both lamina went plastic first at the top and bottom of the panel near the center.

3.6 Plate Strip

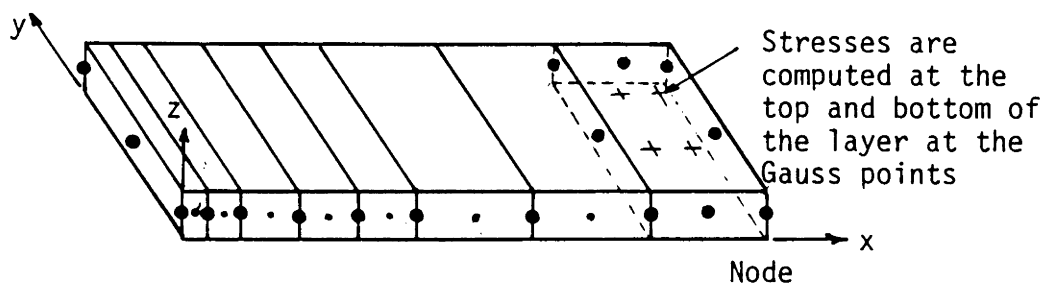
A cantilever plate strip is used to investigate the full geometric and material nonlinear effects on failure analysis. Isotropic, orthotropic, and cross-ply plate strips are examined, with the failure theories being applied to the latter two cases. Also, a two-layer angle-ply ($45^\circ/-45^\circ$) plate strip was analyzed to evaluate the failure criteria. Two layers are used in the analysis, therefore four through-the-thickness constitutive matrices are employed at each Gauss point (see Fig. 3.7).

3.6.1 Isotropic Plate Strip

First, the isotropic plate strip results are discussed. As the load was applied, the Gauss points nearest the wall of the seven element plate strip (see Fig. 3.7), on top and bottom of the structure, exhibit plastic deformation between load values 400 and 600 psi. Based on the magnitude of the scale factor x_m , the Gauss points at the top of the plate went plastic first. As the load was further applied, the material nonlinear effect began to dominate the geometrically nonlinear effect.



(a) Seven element discretization



(b) Eight element discretization

Figure 3.7 Geometry and finite element meshes used in the plate strip problems

Figure 3.8 shows the deflection of the tip of the plate strip as a function of the applied load. When only geometric nonlinearity is included, the plate strip stiffened slightly, and when both nonlinearities are included, a softening is seen to take place. The deformed positions at the maximum load (2,000 psi) are shown in Figure 3.9 for the cases of geometric and geometric/material nonlinear effects. Again, the material effect is clearly present.

Figure 3.10 contains a plot of stress versus load for the same problem. The plot shows the stress predictions at the Gauss points nearest the wall on the bottom of the plate with and without the material nonlinearity. First, notice that the effective stress, $\bar{\sigma}$, is very close to the yield stress at all load levels (5% tolerance was used). Second, the curves show the predicted bending stresses with and without material nonlinear effect. Clearly, for this thick isotropic plate strip, neglecting the material nonlinear effect would be unadvisable as failure would be predicted far too soon based on the geometrically nonlinear description alone. If a thin plate were used, one can argue that the geometric effect will overwhelm the material effect in most cases. This is true, but near failure, the material effect will again emerge.

3.6.2 Orthotropic Plate Strip

The same physical dimensions as those used for the isotropic plate strip are used here, but the mesh now contains eight elements to better define the behavior near the wall. Material type 2 was used.

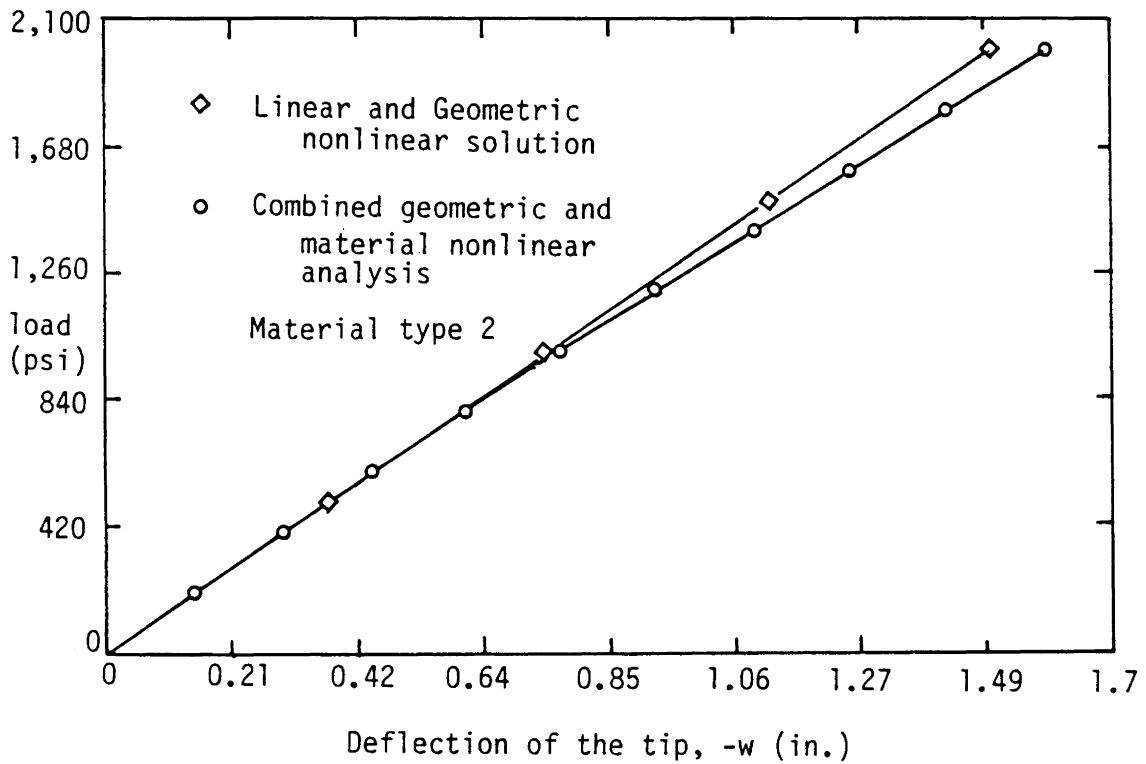


Figure 3.8 Load versus the tip deflection of an isotropic plate strip under uniform load.

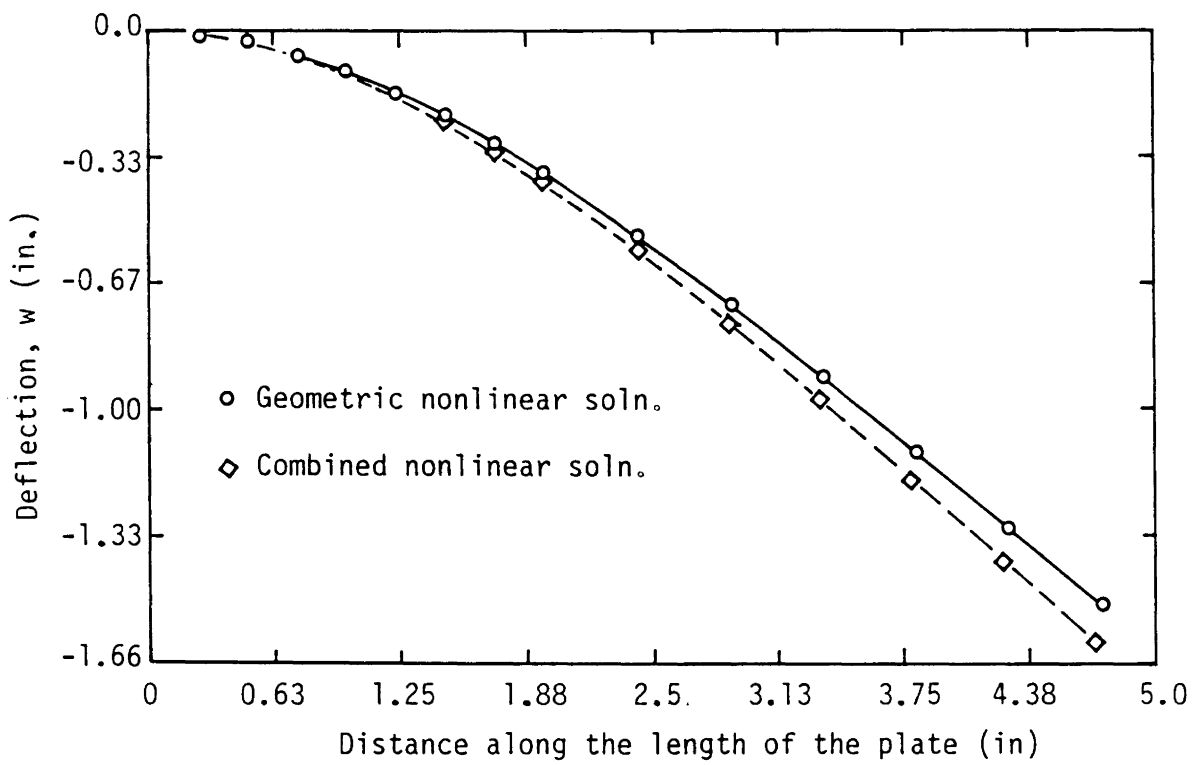


Figure 3.9 Deformed configuration of the isotropic plate strip under uniform pressure (at 2000 psi).

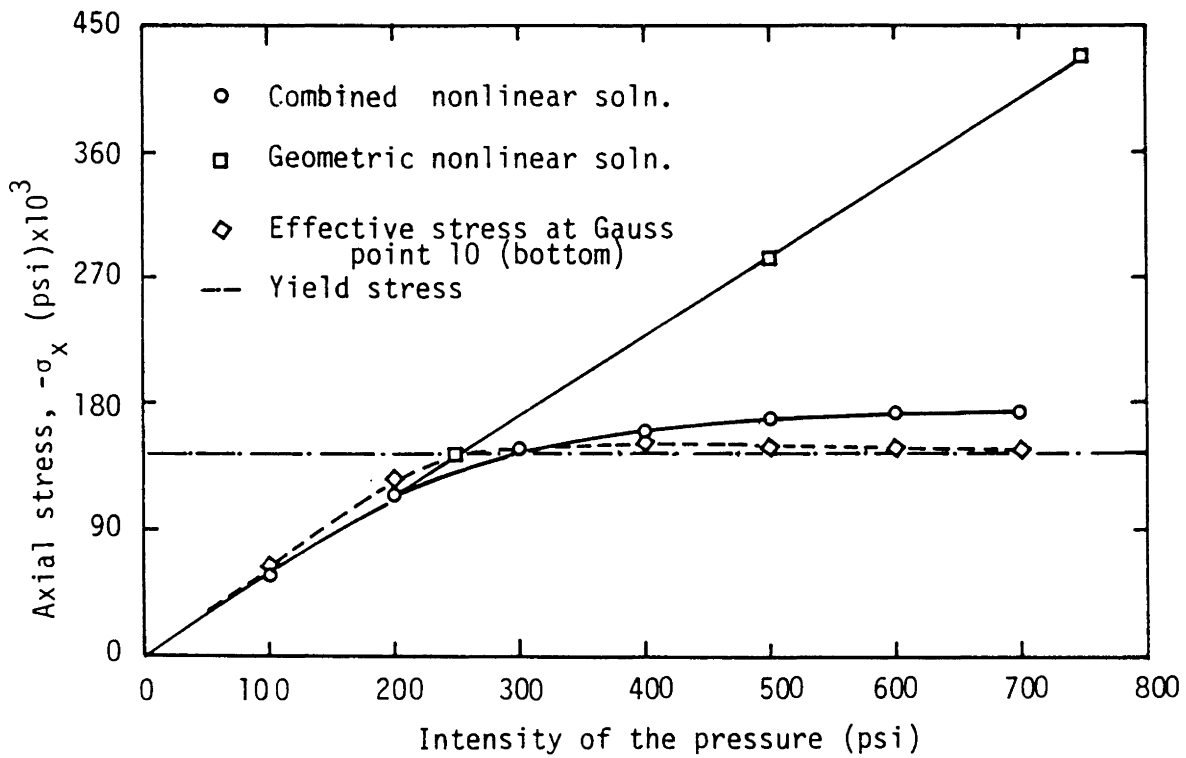


Figure 3.10 Nonlinear effects on the axial stress near the wall of the cantilevered plate strip (isotropic).

The same locations as in the isotropic case go plastic, but they do so at a lower load level. This is due to the weak matrix tensile strength relative to the shear strength of the isotropic materials. Figure 3.11 shows that the overall behavior of the plate strip is linear, even though plasticity occurred early in the load cycle. The bending stresses are much higher in the orthotropic case, and indeed are nearly equal to the fiber tensile strength (200,000 psi) at the 700 psi load level as is seen in Figure 3.12. Therefore, one would expect a nearly linear behavior until a fiber failure occurs. Indeed, this is what is predicted by Hashin's mode criterion when the same loads are used. The plasticity spread to a distance of nearly one inch in the matrix in the x direction before a tensile fiber failure on top and a compressive fiber failure on bottom (near the wall) were predicted at the 700 psi load. After the failure and reduction of these constitutive matrices, the tip deflection was found to be 1.5% greater than the value when no failure was considered. No further load steps were run.

This example was again run using the Tsai-Wu failure criterion. Again, failure was predicted in the same locations, top and bottom of the strip at the wall, but here, the entire constitutive matrix was reduced (as no mode prediction is possible). The solution would not converge after failure with Tsai-Wu because no stiffness at all was left on the top or bottom of the beam, even though fibers were still active in the center. This says that the shear transfer was not sufficient to reroute the loading path through the matrix to the fibers deeper inside the strip. This observation of the distinction between the Hashin and the Tsai-Wu criteria is relative to the model, load steps, and mesh

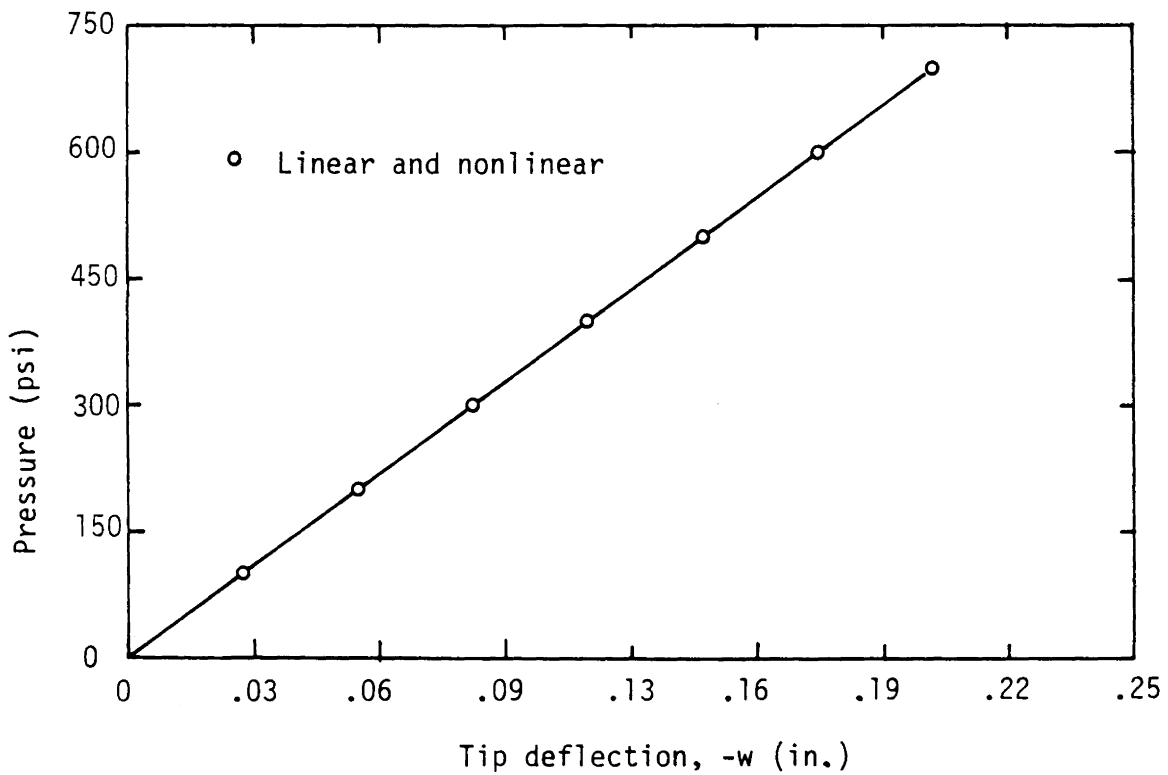


Figure 3.11 Load versus tip deflection of orthotropic plate strip under pressure loading.

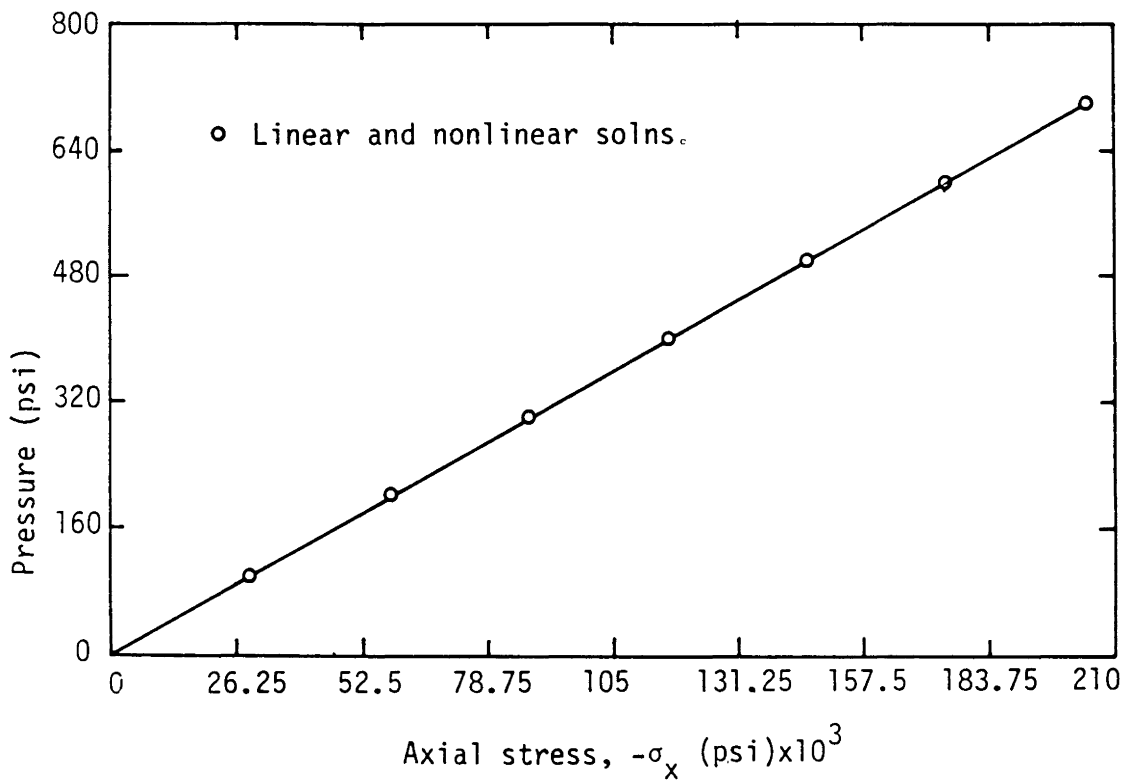


Figure 3.12 Nonlinear effects on the axial (bending) stress near the wall of an orthotropic plate strip.

employed, so that the effect of trying to predict a mode of failure rather than just occurrence of failure can be shown. This only means that using Tsai-Wu a deflection of greater than 1.5% (over the no-failure analysis) at the tip will be experienced and hence greater strains. Leaving the matrix stiffnesses in (i.e. the Hashin criterion) therefore, will start to show different numerical results than when the matrix stiffness must be reduced (i.e. the Tsai-Wu criterion). This results in the possibility of different load paths, and different gross failure modes in examples where the structure geometry is more complex.

3.6.3 Cross-Ply Plate Strip

The same geometry and mesh as in the orthotropic plate strip was used here except that the bottom quarter inch of the strip is made up of a layer of 90° plies. One wouldn't necessarily build this structure in this manner, but it is instructive to look at how failure occurs and what effect plasticity (material nonlinearity) has on it.

Figure 3.13 shows the plot of load versus deflection, which is essentially linear. The loads are much smaller than the orthotropic case as would be expected. The material effect is shown to have a little more influence on the bending stress in the bottom (90°) ply. The bending stress in the upper ply showed no appreciable material effect as in the orthotropic case. Here, plasticity did not occur in the (0°) ply. Plasticity started at the wall at a load of 40 psi and grew to a distance of one and a half inches at the last converged load. Another difference between the cross-ply case and the orthotropic case is that the entire thickness of the (90°) ply went plastic. That

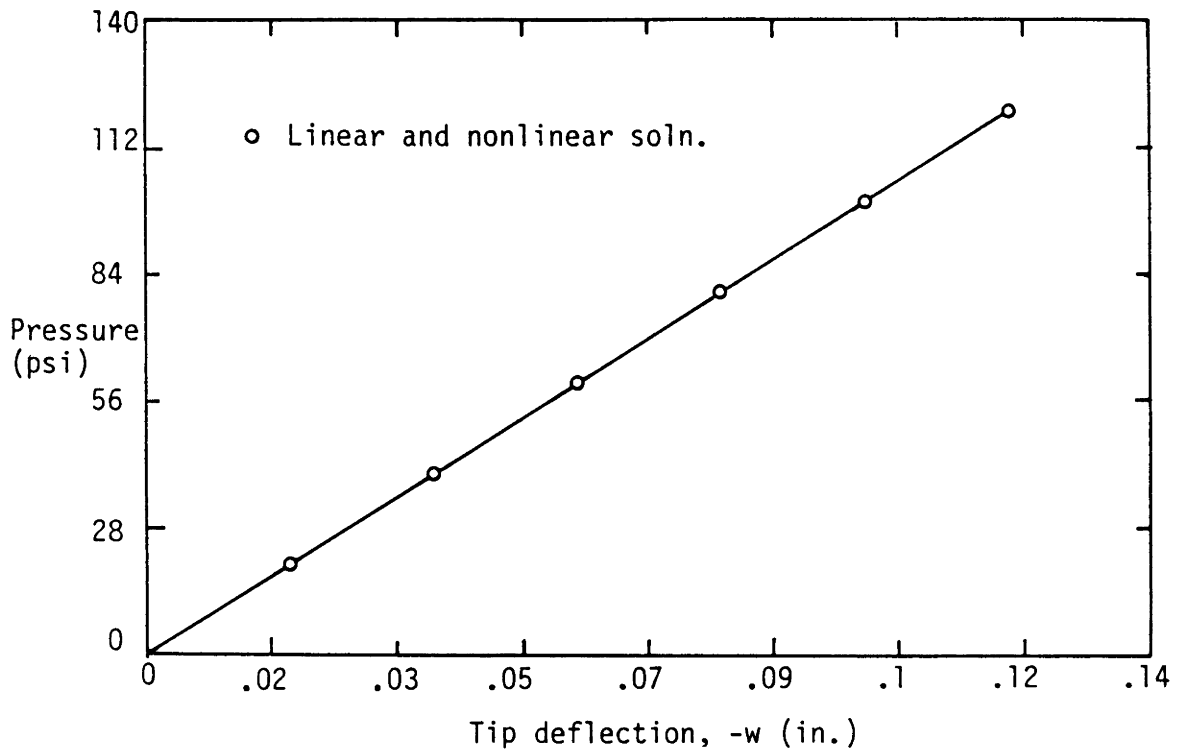


Figure 3.13 Load versus tip deflection of a cross-ply ($0^\circ/90^\circ$) plate strip under pressure load.

is, the bottom quarter inch of the structure for approximately 30% of the strips length was plastic at the last load step. The stresses in the matrix direction in the 90° ply were also over their failure strength, so that one could expect failure before this load level was reached.

Both the Mathers-Hill and the maximum stress criteria predicted failure near the wall in the 90° ply at the 100 psi load level, then farther from the wall at the 120 psi level. The deflections at the tip however, were less than 6% over the case where no failure criterion was employed. Therefore, even though failure was predicted (and the constitutive matrices reduced) for the lower $1/8$ " of the thickness of the strip, the structure does not exhibit noticeable changes in stresses and deflections. Therefore, the load path was not affected very much at all, which is no surprise since the (0°) lamina is on top. The bending stresses on the top do increase, but not dramatically, in taking up the extra load.

3.6.4 Angle Ply ($45^\circ/-45^\circ$) Plate Strip

The thick plate strip used previously to show the effects of the material nonlinearity is used again to evaluate the maximum stress, Tsai-Wu, and Hashin's failure criteria. All stress states are computed using the geometric nonlinearity only. The loading used is the same as before, namely, uniform pressure on the surface at all times. The load step used was 10 psi until first failure occurred, then the computation was terminated.

Both the maximum stress and the Tsai-Wu criteria predicted first failure between 70 and 80 psi of load value at the same locations, at the two Gauss points nearest the wall, top and bottom, and on opposite sides (see Figure 3.14). Hashin's criterion predicted failure at the same load level, but only at the upper Gauss point. The mode of failure is tensile matrix failure in the top lamina. At this same location the maximum stress criterion was violated by a tensile normal stress in the matrix direction (i.e. material x_2 -direction), and σ_2 stress was the largest, as a percentage of its strength, in the Tsai-Wu criterion. At the lower Gauss point, the same phenomenon occurred for the maximum stress and Tsai-Wu criteria, except that the σ_2 stress was now in compression.

The predicted failure locations are consistent with the mechanics of composite material; the corners of the structure where the fibers of each layer are short do not carry much of the load. It is reasonable to expect a matrix failure in these regions. The results indicate this in the corners opposite to where the failure occurred. The fiber is the dominant load carrying member and the normal component of stress in the matrix direction was about half of the value predicted at the failed locations.

It is interesting to note that a noninteracting (no products of different stress components) stress criterion (maximum stress) and an interacting stress criterion (Tsai-Wu) predict failure at the same load levels, both in compression and tension, at the same locations in the structure. Recall that the interaction term, F_{12} , was set to zero in the Tsai-Wu criterion, effectively taking away the stress interaction in

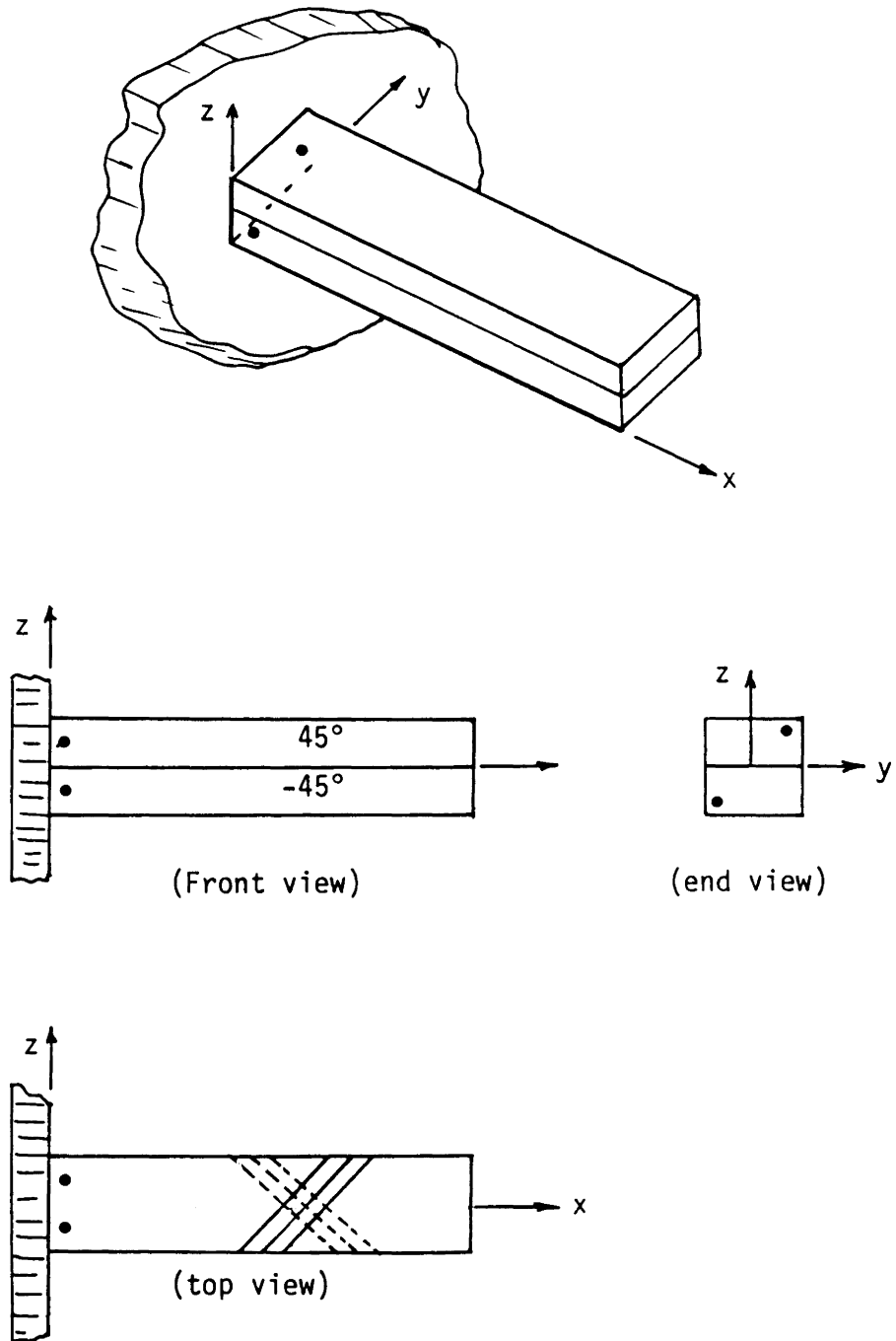


Figure 3.14 First failure locations in the angle-ply plate strip.

the explicit sense (the stress interaction is still preserved implicitly by the form of the tensor polynomial, e.g. the failure envelope is still three dimensional with curved surfaces in stress space).

Of even greater interest is the fact that Hashin's criterion predicted only the tensile matrix failure, and not the compressive matrix failure. This is due to the fact that for a compressive matrix failure another term involving the in-plane and transverse shear strengths is involved (transverse isotropy in the plane perpendicular to the fibers is assumed). In the case of a nearly isotropic material, this term is almost zero and one would expect tensile and compressive failures to occur at nearly the same load level. As the transverse shear strength (F_{23}) gets larger relative to the in-plane shear strength (F_{12}), a larger compressive matrix normal stress component (σ_2) is needed for failure to occur. The same stress component (σ_2) would predict failure at lower magnitude if it were tension. This is one of the "physical reasoning" points Hashin brings out in his criterion; it should take more stress to compress a matrix to failure than it does to pull a matrix to failure. The present example illustrates this point.

CHAPTER 4

SUMMARY AND CONCLUSIONS

4.1 General Comments

A finite element computational procedure is developed to analyze laminated composite structures undergoing large deformations and experiencing elastic-plastic behavior. The finite element model is based on the total Lagrangian, incremental formulation of 3-D elasticity with some simplifying assumptions concerning the thickness variations. The modified Hill's criterion is used to determine plastic deformation and reduce the material stiffness coefficients. Several failure criteria, including the maximum stress, Tsai-Wu, and Hashin criteria are also included in the computational scheme. The criteria can be used to predict first-ply and post-first-ply failure of composite laminates. The element developed is very general in that it can be used for modelling of complex geometries (plates and shells), orthotropic and anisotropic materials, and different types of mechanical loads. The element is used to determine the load-deflection behavior with and without geometric and/or material nonlinear effects. While the element is capable of modelling more complex geometries, laminates and loadings, the primary objective of this study was to develop the procedure, validate it and illustrate its use in the analysis of simple problems. This objective was successfully achieved. Some observations concerning geometric nonlinearity, material nonlinearity and failure criteria are presented in the following sections.

4.2 Geometric and Material Nonlinear Effects

For plate and shell structures, in general, the material nonlinearity is important when the side-to-thickness ratio of the structure becomes small, and the geometric nonlinearity is important when the ratio is large. Thus, each nonlinearity is dominant in different problems, and both are important in most problems undergoing large deformations.

For laminated anisotropic structures, the material nonlinearity is insignificant in both thick and thin cases. The matrix material becomes plastic, but the fibers do not, and since a properly designed structure has the fibers carrying the load as much as possible, the material nonlinear effect, due to static loading, is negligible. The material nonlinear effects due to thermal loads, for example, are known to play a much more significant role than what the material nonlinear effect due to static loading seems to have on composite structures made of unidirectional composite laminae.

4.3 Failure Criteria

The four failure theories used in this study varied from an energy description (derivable) to a stress space criterion (physical). Each of these depend on the computed stress state in material coordinates and each of them predicted failure for the orthotropic and cross-ply plate strip examples at comparable locations and at comparable load levels. For these two examples, any of the four criteria would be appropriate to use, with the logical choice being Hashin's criterion because it predicts more information about the the mode of failure. For the angle-

ply example, where only geometric nonlinear effects were employed, again the maximum stress, Tsai-Wu, and Hashin criteria all predicted the same load level for failure and the same locations (Hashin's theory predicting only tensile matrix failure). The big difference in the angle-ply and cross-ply cases is that a matrix failure is predicted in angle-ply plates whereas in the orthotropic and cross-ply cases a fiber failure is predicted.

The material nonlinear effect may have an important role to play in the angle-ply case, as the plastic action of the matrix could increase the failure load to a point where the fibers will fail. In this case however, elastic unloading needs to be incorporated into the material nonlinear scheme so that the matrix has a chance to increase its stiffness when a negative effective plastic strain increment is arrived at. Recall, this study is based only on stresses, and assumes the strains computed are allowed by the structure.

4.4 Recommendations

As discussed earlier, the element can be used to solve much more general problems than the sample problems discussed in this study. Application of the element to laminated shell structures under mechanical and thermal loads is awaiting. Development of a preprocessor or interfacing the program with a general purpose computer program would allow the solution of more practical geometries.

It would be interesting to see the elastic unloading incorporated into the material nonlinear scheme used in this study, and then use that improved model to compare with some of the other material nonlinear

models for anisotropic structures, for example, where matrix failure is known to occur.

REFERENCES

1. Chang, T. Y. and Sawamiphakdi, K., "Large Deformation Analysis of Laminated Shells by Finite Element Method," Computers and Structures, Vol. 13, pp. 331-340, 1981.
2. Chao, W. C. and Reddy, J. N., "Analysis of Laminated Composite Shells using a Degenerated 3-D Element," International J. Numer. Mechanical Engineering, Vol. 20, pp. 1991-2007, 1984.
3. Chandrashakara, K. and Reddy, J. N., "Nonlinear Analysis of Composite Laminates Accounting for Elastic-Plastic Material Behavior," Proc. Int. Symp. on Composite Materials and Structures, Beijing, China, June 10-13, 1986.
4. Parisheh, H., "Large Displacements of Shells Including Material Nonlinearities," Computer Methods in Applied Mechanics and Engineering, Vol. 27, pp. 183-214, 1981.
5. Ramm, E. and Satteler, J. M., "Elastoplastic Large Deformation Shell Analysis Using Degenerated Elements," in Nonlinear Finite Element Analysis of Plates and Shells, edited by T. J. R. Hughes, A. Pifko and A. Jay, AMD-48, ASME, pp. 265-282, 1981.
6. Whang, B., "Elasto-Plastic Orthotropic Plates and Shells," Proc. Symposium on Application of F.E.M. in Civil Engineering, Vanderbilt University, Tennessee, 1969.
7. Owen, D. R. J., and Figueiras, J. A., "Elasto Plastic Analysis of Anisotropic Plates and Shells by the Semiloof Element," International Journal of Numerical Methods in Engineering, Vol. 19, pp. 521-539, 1983.
8. Adams, D. F., "Inelastic Analysis of a Unidirectional Composite Subjected to Transverse Normal Loading," Journal of Composite Materials, Vol. 4, pp. 310-328, 1970.
9. Foye, R. L., "Theoretical Post-Yielding Behavior of Composite Laminates. Part I - Inelastic Micromechanics," Journal of Composite Materials, Vol. 7, pp. 178-193, 1973.
10. Valliapan, S., Boonlualohr, P. and Lee, I. K., "Non-linear Analysis for Anisotropic Materials," International Journal for Numerical Methods in Engineering, Vol. 10, pp. 597-606, 1976.
11. Mulhern, J. F., Roger, T. G. and Spencer, A. J. M., "A Continuum Model for Fibre-Reinforced Plastic Materials," Proc. Roy. Soc., Series A, Vol. 301, p. 473, 1967.

12. Mulhern, J. F., Roger, T. G. and Spencer, A. J. M., "Cyclic Extension of an Elastic Fibre with an Elastic-Plastic Coating," J. Inst. Maths. Applics., Vol. 3, p. 21, 1967.
13. Hill, R., "Theory of Mechanical Properties of Fiber-Strengthened Materials: II. Inelastic Behavior," J. Mech. Phys. Solids, Vol. 12, p. 213, 1964.
14. Mulhern, J. F., Roger, T. G. and Spencer, A. J. M., "A Continuum Theory of a Plastic-Elastic Fibre-Reinforced Material," Int. J. Engr. Sci., Vol. 7, p. 129, 1969.
15. Spencer, A. J. M., "A Continuum Theory of a Plastic-Rigid Solid Reinforced by Two Families of Inextensible Fibres," Q. J. Mech. Appl. Math., Vol. 23, p. 489, 1970.
16. Spencer, A. J. M., "Dynamics of Ideal Fibre-Reinforced Rigid-Plastic Beams," J. Mech. Phys. Solids, Vol. 22, p. 147, 1974.
17. Pipkin, A. C. and Rogers, T. G., "Plane Deformations of Incompressible Fiber-reinforced Materials," J. Appl. Mech., Vol. 38, p. 634, 1971.
18. Rogers, T. G. and Pipkin, A. C., "Small Deflections of Fiber-Reinforced Beams and Slabs," J. Appl. Mech., Vol. 38, p. 1047, 1971.
19. Dvorak, G. J., Rao, M. S. M. and Tarn, J. Q., "Yielding in Unidirectional Composites Under External Loads and Temperature Changes," J. Composite Materials, Vol. 7, p. 194, 1973.
20. Dvorak, G. J., Rao, M. S. M. and Tarn, J. Q., "Generalized Initial Yield Surfaces for Unidirectional Composites," J. Appl. Mech., Vol. 41, p. 249, 1974.
21. Dvorak, G. J. and Rao, M. S. M., "Axisymmetric Plasticity Theory of Fibrous Composites," Int. J. Engng. Sci., Vol. 14, p. 361, 1976.
22. Dvorak, G. J. and Rao, M. S. M., "Thermal Stress in Heat-Treated Fibrous Composites," J. Appl. Mech., Vol. 43, p. 619, 1976.
23. Dvorak, G. J. and Bahei-El-Din, Y. A., "Elastic-Plastic Behavior of Fibrous Composites," J. Mech. Phys. Solids, Vol. 27, p. 51, 1979.
24. Dvorak, G. J. and Bahei-El-Din, Y. A., "Plasticity of Composite Laminates," Proceedings of the Research Workshop on Mechanics of Composite Materials, Dvorak, G. J., ed., Duke University, p. 32, October 1978.
25. Dvorak, G. J. and Bahei-El-Din, Y. A., "Plasticity Analysis of Fibrous Composites," J. Appl. Mech., Vol. 49, p. 327, 1982.

26. Bahei-El-Din, Y. A., Dvorak, G. J. and Utku, S., "Finite Element Analysis of Elastic-Plastic Fibrous Composite Structures," Computers and Structures, Vol. 13, p. 321, 1981.
27. Bahei-El-Din, Y. A. and Dvorak, G. J., "Plastic Yielding at a Circular Hole in a Laminated FP-Al Plate," Modern Development in Composite Materials and Structures, Vinson, J. R., ed., The American Society of Mechanical Engineers, p. 123, 1979.
28. Bahei-El-Din, Y. A. and Dvorak, G. J., "Plasticity Analysis of Laminated Composite Plates," J. Appl. Mech., Vol. 49, p. 740, 1982.
29. Hutchinson, J. W., "Elastic-Plastic Behavior of Polycrystalline Metals and Composites," Proc. Roy. Soc., Series A, Vol. 319, p. 247, 1970.
30. Bahei-El-Din, Y. A., "Plasticity Analysis of Metal-Matrix Composite Laminates," Ph.D. Dissertation, Duke University, 1979.
31. Lou, Y. C. and Schapery, R. A., "Viscoelastic Characterization of a Nonlinear Fiber-Reinforced Plastic," J. Composite Materials, Vol. 5, p. 208, April 1971.
32. Rao, M. S. M., "Plasticity Theory of Fiber-Reinforced Metal Matrix Composites," Ph.D. Dissertation, Duke University, 1974.
33. Hoffman, O., "A Continuum Model for the Engineering Analysis of Metal Matrix Composites," Modern Development in Composite Materials and Structures, Vinson, J. R., ed., The American Society of Mechanical Engineers, p. 101, 1979.
34. Min, K. B., "A Plain Stress Formulation for Elastic-Plastic Deformation of Unidirectional Composites," J. Mech. Phys. Solids, Vol. 29, p. 327, 1981.
35. Min, K. B. and Crossman, F. W., "History-Dependent Thermomechanical Properties of Graphite/Aluminum Unidirectional Composites," Composite Materials: testing and Design (Sixth Conference), ASTM STP 787, Daniel, I. M., ed., American Society for Testing and Materials, p. 371, 1982.
36. Min, K. B. and Flaggs, D. L., "A Non-Isothermal Plasticity Analysis of Composite Laminates," Mechanics of Composite Materials - 1983, Proceedings of the Symposium, Boston, MA, November 13-18, 1983, American Society of Mechanical Engineers, P. 51.
37. Min, K. B. and Flaggs, D. L., "A Thermomechanical Elastoplastic Analysis of Fibrous Composite Laminates," Lockheed Aircraft Co., Sunnyvale, CA, 1985.

38. Hunsaker, B., Jr., Vaughan, D. K., Stricklin, J. A. and Haisler, W. E., "A Comparison of Current Work-Hardening Models Used in the Analysis of Plastic Deformation," TEES-RPT-2926-73-3, October 1973, Aerospace Engineering Department, Texas A&M University, College Station, Texas.
39. Filippa, C. A., "Procedures for Computer Analysis of Large Nonlinear Structural Systems," Large Engineering Systems, Wexler, A., ed., Pergamon Press, p. 60, 1976.
40. Wolf, E. G., Min, K. B. and Kural, M. H., "Thermal Cycling of a Unidirectional Graphite/Magnesium Composites," J. Materials Science, Vol. 20, p. 1141, April 1985.
41. Ruffin, A. C., Rimbois, P. G. and Bigelow, S. D., "Point-Stress Analysis of Continuous Fiber-Reinforced Composite Materials With an Elastic-Plastic Matrix," Computers and Structures, Vol. 20, p. 375, 1985.
42. Aboudi, J., "A Continuum Theory for Fiber-Reinforced Elastic-Viscoplastic Composites," Int. J. Engng. Sci., Vol. 20, p. 605, 1982.
43. Aboudi, J., "Effective Behavior of Inelastic Fiber-Reinforced Composites," Int. J. Engng. Sci., Vol. 22, p. 439, 1984.
44. Aboudi, J., "The Effective Thermomechanical Behavior of Inelastic Fiber-Reinforced Materials," Int. J. Engng. Sci., Vol. 23, p. 773, 1985.
45. Aboudi, J. and Benveniste, Y., "Constitutive Relations for Fiber-Reinforced Inelastic Laminated Plates," J. Appl. Mech., Vol. 51, p. 107, 1984.
46. Petit, P. H. and Waddoups, M. E., "A of Predicting the Nonlinear Behavior of Laminated Composites," J. Composite Materials, Vol. 3, p. 2, 1969.
47. Hahn, H. T. and Tsai, S. W., "Nonlinear Elastic Behavior of Unidirectional Composite Laminae," J. Composite Materials, Vol. 7, p. 102, 1973.
48. Hahn, H. T., "Nonlinear Behavior of Laminated Composites," J. Composite Materials. Vol. 7, p. 257, 1973.
49. Hill, R., "A Theory of the Yielding and Plastic Flow of Anisotropic Metals," Proc. Roy. Soc., Vol. 193, No. 1033, p. 189, 1948.
50. Hill, R., The Mathematical Theory of Plasticity, Oxford University Press, 1956.

51. Hu, L. W., "Studies on Plastic Flow of Anisotropic Metals," J. Appl. Mech., September 1956.
52. Jensen, W. R., Falby, W. E. and Prince, N., "Matrix Analysis for Anisotropic Inelastic Materials," AFFDL-TR-65-220, 1966.
53. Dubey, R. N. and Hillier, M. J., "Yield Criteria and Bauschinger Effect for a Plastic Solid," J. Basic Engineering, Paper No. 711-MET-p., March 1972.
54. Shih, C. F. and Lee, D., "Further Developments in Anisotropic Plasticity," J. Engineering Materials and Technology, Vol. 100, p. 294, July 1978.
55. Pifko, P., Levine, H. S. and Armen, H., Jr., "PLANS-A Finite Element Program for Nonlinear Analysis of Structures," NASA CR-2568, 1975.
56. Renieri, G. D. and Herakovich, C. T., "Nonlinear Analysis of Laminated Fibrous Composites," VPI-E-76-10, Engineering Science and Mechanics Department, Virginia Polytechnic Institute and State University, Blacksburg, Virginia, 1976.
57. Griffin, O. H., Jr., Kamat, M. P. and Herakovich, C. T., "Three-Dimensional Analysis of Laminated Composites," J. Composite Materials, Vol. 15, p. 543, November 1981.
58. Hill, R., "A Theory of the Yielding and Plastic Flow of Anisotropic Metals," Proceedures of the Royal Society of London, Series A, Vol. 193, pp. 281-297, 1948.
59. Tsai, S. W., "Strength Characteristics of Composite Materials," NASA CR-224, 1965.
60. Mathers, M. D. and Razzaque, A., FE2000 Manual, Numeric Corp., 1985.
61. Tsai, S. W. and Wu, E. M., "A General Theory of Strength for Anisotropic Materials," Journal of Composite Materials, Vol. 5, p. 58, 1971.
62. Goldenblat, I. and Kopnov, V. A., "Strength of Glass Reinforced Plastics in the Complex Stress State," Mekhanika Polymerov, Vol. 1, p. 70, 1965. English Translation: Polymer Mechanics, Vol. 1, p. 54, 1966.
63. Tennyson, R. C., MacDonald D. and Nanyaro, A. P., "Evaluation of the Tensor Polynomial Failure Criterion for Composite Materials," Journal of Composite Materials, Vol. 12, pp. 63-75, 1977.

64. Puppo, A. H. and Evenson, H. A., "Strength of Anisotropic Materials Under Combined Stresses," AIAA/ASME 12th Structures, Structural Dynamics and Materials Conference, April 19-21, 1971.
65. Hashin, Z., Theory of Fiber Reinforced Materials, NASA CR-1974, March 1972.
66. Bathe, K. J., Ramm E. and Wilson, E. C., "Finite Element Formulations for Large Deformation Dynamic Analysis," International Journal Numer. Methods in Engineering, Vol. 9, pp. 353-386, 1975.
67. Reddy, J. N., Energy and Variational Methods in Applied Mechanics, Wiley, New York, 1984.
68. Malvern, L. E., Introduction to the Mechanics of a Continuous Medium, Prentice-Hall, Englewood Cliffs, N.J., 1974.
69. Zienkiewicz, O. C., The Finite Element Method in Engineering Science, McGraw-Hill, London, 1971.
70. Reddy, J. N., An Introduction to the Finite Element Method, McGraw-Hill, New York, 1984.

APPENDIX A

MATERIAL PROPERTIES USED IN THIS STUDY

(a) Type 1, Isotropic, Perfectly Plastic (psi, in/in)

<u>Yield Point</u>		<u>First Plastic Point</u>	
<u>Stresses (psi)</u>	<u>Strains (in/in)</u>	<u>Stresses (psi)</u>	<u>Strains (in/in)</u>
$\sigma_1 = 144,000$	$\epsilon_1 = .0144$	$\sigma_1 = 144,000$	$\epsilon_1 = .0184$
$\sigma_2 = 144,000$	$\epsilon_2 = .0144$	$\sigma_2 = 144,000$	$\epsilon_2 = .0184$
$\sigma_{45} = 144,000$	$\epsilon_{45} = .0144$	$\sigma_{45} = 144,000$	$\epsilon_{45} = .0184$
$\sigma_{12} = 83,138$	$\gamma_{12} = .02385$	$\sigma_{12} = 83,138$	$\gamma_{12} = .02785$
$\sigma_{13} = 83,138$	$\gamma_{13} = .02385$	$\sigma_{13} = 83,138$	$\gamma_{13} = .02785$
$\sigma_{23} = 83,138$	$\gamma_{23} = .02385$	$\sigma_{23} = 83,138$	$\gamma_{23} = .02785$

Original Constitutive Properties

$$E_1 = 10^7 \text{ psi}$$

$$E_2 = 10^7 \text{ psi}$$

$$G_{12} = 3,846 \times 10^6 \text{ psi}$$

$$G_{13} = 3,846 \times 10^6 \text{ psi}$$

$$G_{23} = 3,846 \times 10^6 \text{ psi}$$

$$\nu_{12} = 0.30$$

Strengths (in psi)

$$1T = 144,000$$

$$1C = -144,000$$

$$2T = 144,000$$

$$2C = -144,000$$

$$12 = 83,138$$

$$13 = 83,138$$

$$23 = 83,138$$

(b) Type 2, Boron-Epoxy

<u>Yield Point</u>		<u>First Plastic Point</u>	
Stresses (psi)	Strains (in/in)	Stresses (psi)	Strains (in/in)
$\sigma_1 = 120,000$	$\epsilon_1 = .004$	$\sigma_1 = 160,000$	$\epsilon_1 = .0054$
$\sigma_2 = 8,500$	$\epsilon_2 = .0031$	$\sigma_2 = 20,000$	$\epsilon_2 = .0103$
$\sigma_{45} = 6,600$	$\epsilon_{45} = .0024$	$\sigma_{45} = 10,000$	$\epsilon_{45} = .0034$
$\sigma_{12} = 5,000$	$\gamma_{12} = .007$	$\sigma_{12} = 12,800$	$\gamma_{12} = .0221$
$\sigma_{13} = 5,000$	$\gamma_{13} = .007$	$\sigma_{13} = 12,800$	$\gamma_{13} = .0221$
$\sigma_{23} = 3,571$	$\gamma_{23} = .007$	$\sigma_{23} = 9,143$	$\gamma_{23} = .0221$

Original Constitutive Properties

$$E_1 = 30 \times 10^6 \text{ psi}$$

$$E_2 = 2.7 \times 10^6 \text{ psi}$$

$$G_{12} = 0.7 \times 10^6 \text{ psi}$$

$$G_{13} = 0.7 \times 10^6 \text{ psi}$$

$$G_{23} = 0.5 \times 10^6 \text{ psi}$$

$$\nu_{12} = 0.21$$

Strengths (in psi)

$$1T = 200,000$$

$$1C = -200,000$$

$$2T = 12,500$$

$$2C = -12,500$$

$$12 = 19,000$$

$$13 = 19,000$$

$$23 = 13,800$$

(c) Type 3, Isotropic II

$$E = 30 \times 10^6 \text{ psi}$$

$$\nu = 0.30$$

(d) Type 4, Unnamed Orthotropic

$$E_1 = 25,000 \text{ N/mm}^2$$

$$E_2 = 2,000 \text{ N/mm}^2$$

$$G_{12} = 10,000 \text{ N/mm}^2$$

$$G_{13} = 10,000 \text{ N/mm}^2$$

$$G_{23} = 4,000 \text{ N/mm}^2$$

$$\nu_{12} = 0.275 \text{ N/mm}^2$$

(e) Type 5, Isotropic III

$$E = 2,000 \text{ N/mm}^2 \quad \nu = 0.3$$

(f) Type 6, Isotropic IV

$$E = 3,103 \text{ N/mm}^2 \quad \nu = 0.3$$

(g) Type 7, Isotropic

Same as Type 1 except $144,000 \rightarrow 25,000$ and $83,138 \rightarrow 14,434$.

**The vita has been removed from
the scanned document**